DEUTSCHES ELEKTRONEN-SYNCHROTRON DESY

DESY 79/84
December 1979

RECENT RESULTS FROM PETRA

by

B. H. Wiik

Invited Talk given at the Meeting of The Division of Particle Physics of The American Physical Society, McGill University, Montreal, Canada, 25 - 27 October 1979

NOTKESTRASSE 85 · 2 HAMBURG 52

To be sure that your preprints are promptly included in the
HIGH ENERGY PHYSICS INDEX ,
send them to the following address (if possible by air mail) :

DESY
Bibliothek
Notkestrasse 85
2 Hamburg 52
Germany

DESY 79/84
December 1979

RECENT RESULTS FROM PETRA

B.H.Wiik
Deutsches Elektronen-Synchrotron DESY, Hamburg, Germany,
Notkestrasse 85 - 2000 Hamburg 52 - Germany

1. INTRODUCTION

The experimental program at the new DESY electron-positron storage ring PETRA[1] got underway late 1978, more than half a year ahead of schedule. Initially data[2] were collected at c.m. energies of 13 GeV, 17 GeV and 27.4 GeV using three large detectors MARK J, PLUTO and TASSO. In June of 1979 a fourth detector, JADE, was installed and these detectors have since taken data at c.m. energies between 22 GeV and 31.6 GeV, the highest energy available with the present complement of klystrons. The energy region between 29.5 GeV and 31.6 GeV, have been scanned in steps of 20 MeV in a search for narrow 1^{--} states.

Several new results have been obtained during the first year of data taking:

The data on various QED processes agree with the theoretical predictions down to distances of $2 \cdot 10^{-16}$ c.m. and confirm lepton universality at small distances.

The data on multihadron final states give clear evidence for jets and they show that the threshold for $t\bar{t}$ production, where t is a quark with charge 2/3 e, must be above 31.5 GeV.

The outstanding experimental result has been the observation of three-jet events, first seen[3,4] by the TASSO Collaboration and since confirmed[5,6,7] by all the other groups. Such events are evidence for hard gluon bremsstrahlung which is expected in any field theory of strong interactions.

The first data on $e^+e^- \to e^+e^-$ hadrons at high energies have been obtained by the PLUTO Collaboration.

In this talk I'll first describe the status of PETRA and then discuss these experimental results in more detail.

2. STATUS OF PETRA

A schematic layout of the DESY accelerator complex is shown in Fig. 1. PETRA (= Positron Elektron Tandem Ring Anlage) is made of eight 45° bends joined by eight straight sections, four 108 m long and four 68.4 m long. The total circumference is 2.3 km. Electrons are injected from the DESY synchrotron directly into PETRA, the positrons are first accumulated in a small storage ring PIA and then injected into PETRA via DESY.

The energy and luminosity of PETRA has been climbing from 13 GeV and a peak luminosity of 2×10^{29} $cm^{-2}sec^{-1}$ at the beginning of the year to 31.6 GeV and 5×10^{30} $cm^{-2}sec^{-1}$. This luminosity should be compared to a predicted maximum luminosity of 2.2×10^{31} $cm^{-2}sec^{-1}$ for 2 bunches of positrons colliding with 2 bunches of electrons and a free distance of $\pm$ 7.5 m in the interaction region between the quadrupoles. On the average, an integrated luminosity

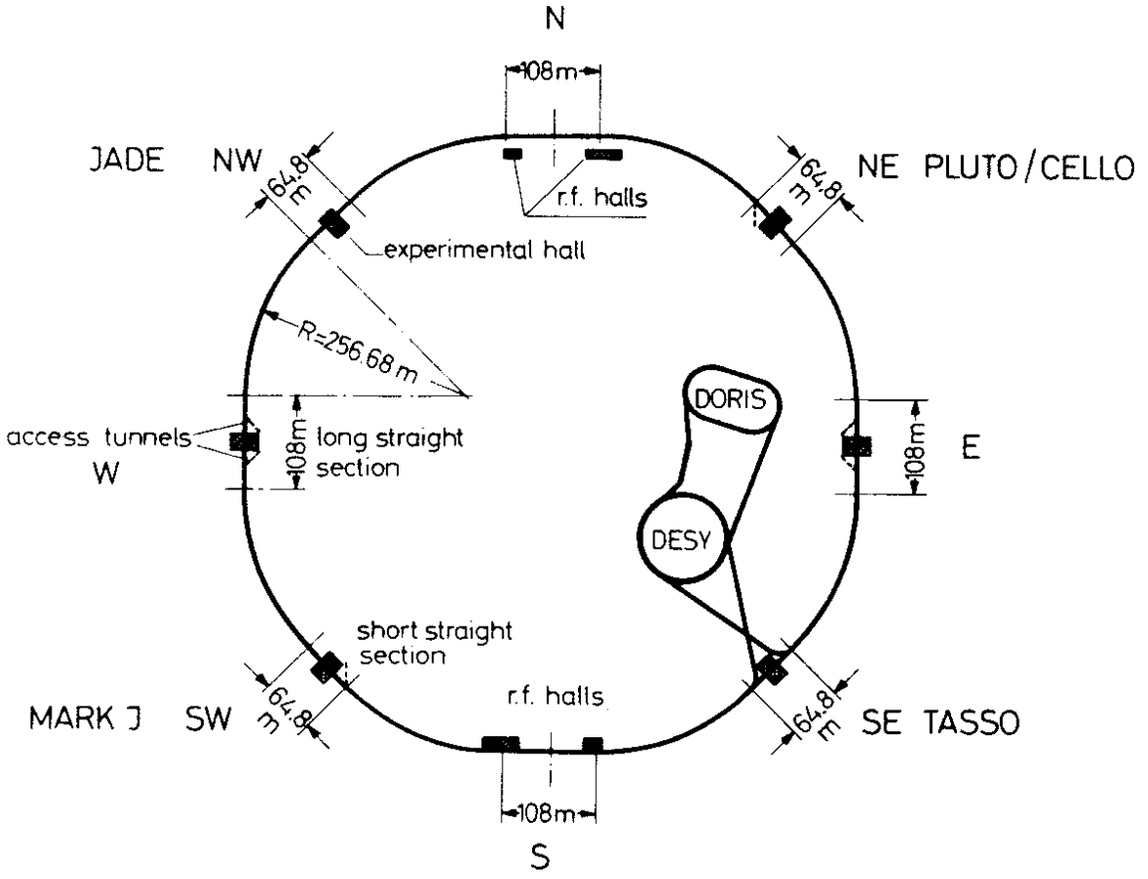

Fig. 1 - Layout of the DESY accelerators

of about 100 nb^{-1} per day is obtained at 30 GeV, this corresponds to some 25 hadron events per day.

The circulating electron beams radiate and this leads to a build up of transverse polarization with atime constant[8] $\tau = 98.8\text{sec}\ (R\rho^2/E^5)$. R and ρ are the geometrical and the bend radia in meters respectively, and E the beam energy in GeV. From this equation, at a beam energy of 15 GeV, we predict a polarization time τ of about 30 min. Since this time constant is short compared to the storage time we expect, in absence of strong depolarization effects, that the beams are polarized. A measurement of $e^+e^- \to q\bar{q}$ can be used to determine the degree of polarization. The distribution of the jet axis, assuming the quarks to be fermions, is given by

$$\frac{d\sigma}{d\Omega} \sim 1 + \cos^2\theta + P^2 \sin^2\theta \cdot \cos 2(\phi - \Delta) \qquad (1)$$

where p is the degree of transverse polarization and Δ a possible angle in the interaction region between the polarization vector and the transverse direction. θ and ϕ denotes the production and azimuthal angle. The azimuthal distribution of 2-jet events observed by the JADE Collaboration and selected using thrust (see below) is plotted in Fig. 2. The data show a strong azimuthal dependence and a fit to the form given above yields $\Delta = -10^{\circ} \pm 14^{\circ}$ and $p = 0.85 \pm 0.14$.

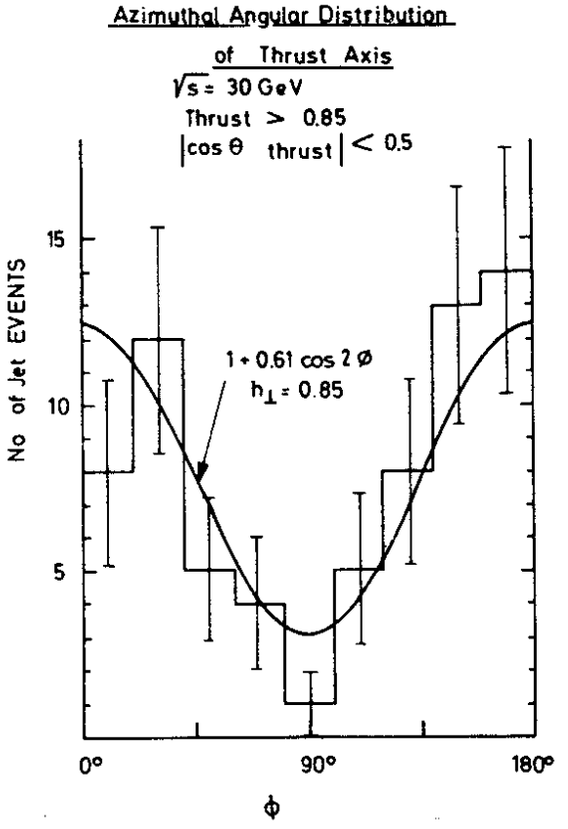

Fig. 2 - Azimuthal distribution of the jet axis in two-jet events as measured by JADE at 30 GeV in c.m.

During the long shut down at the end of the year the number of r.f. cavities will be increased from 32 to 64 and the r.f. power will be doubeled. With this r.f.system PETRA will be able to explore energies up to 38 GeV in c.m. Some of the PETRA parameters are listed in table I.

Table I - PETRA parameters

Maximum c.m. energy:	32 GeV (38 GeV early 1980)
Average circulating current:	$\sim$ 8 mA/Ring
Number of Bunches:	2/Ring (4 possible)
Luminosity after fill:	$5 \times 10^{30} cm^{-2} sec^{-1}$ at 30.0 GeV
Tune shift Q_V^{max}, Q_H^{max}:	0.027 / Interaction Region
Lifetime:	$\sim$ 6.5 hours just after filling $\sim$ 24 hours towards the end of the fill

Table I (continued)

Number of interaction regions:	4 (can be extended to 6)
Length of interaction region:	15 m
Interaction volume:	$\sigma_t \leq 0.07$ cm at 14 GeV $\sigma_L \gtrsim 3$ cm
Vacuum in the interaction regions:	$\sim 10^{-9}$ torr after fill $\sim 10^{-10}$ torr towards the end of the fill

There are four interaction regions equipped with experiments:

SE TASSO Collaboration
Aachen, Bonn, DESY, Hamburg, I.C.London, Oxford, Rutherford, Weizmann and Wisconsin
Large conventional solenoid. Central part with tracking chambers and time of flight counters completed. The muon chambers are installed. The hadron arms are nearly completed and the liquid Argon detector will be installed later this year and in 1980.

NE PLUTO Collaboration
Aachen, Bergen, DESY, Hamburg, Maryland, Siegen, Wuppertal
This is a modified version of the superconducting magnetic solenoid detector which collected data at DORIS. In particular the muon and electron detection have been much improved. This detector is now taking data but will presumably be replaced by the CELLO detector during the long shutdown at the end of the year.

CELLO Collaboration
DESY, Karlsruhe, Munich, Orsay, Paris, Saclay
Superconducting solenoid filled with tracking chambers and surrounded by a liquid Argon detector

NW JADE Collaboration
Daresbury, DESY, Hamburg, Heidelberg, Lancaster, Manchester, Tokyo
Conventional solenoid with a high pressure drift chamber as a tracking detector. Particles are identified by measurements of dE/dx. Large leadglass photon detector mounted outside the solenoid. This detector was installed in June.

SW MARK J Collaboration
Aachen, DESY, MIT, NIKEF Amsterdam, Peking
This detector is a fine grained calorimeter well suited to measure electrons, muons and the energy flow of hadrons.

3. TEST OF QED AND RELATED TOPICS

Electron-positron colliding beams make it possible to test the structure of quantum-electrodynamics at very high momentum transfer in a clean environment with negligible corrections due to strong interactions.

So far the following reactions have been investigated:

1) $e^+e^- \rightarrow e^+e^-$ [7,9,10]

2) $e^+e^- \rightarrow \mu^+\mu^-$ [9]

3) $e^+e^- \to \tau^+\tau^-$ [9]

4) $e^+e^- \to \gamma\gamma$ [7]

5) $e^+e^- \to e^+e^-\mu^+\mu^-$ [9], $e^+e^- \to e^+e^-(\mu^+\mu^- + e^+e^-)$ [10]

Reactions 1 - 4 are proportional to α^2 and decreases with energy as $1/s$ - i.e. $sd\sigma/d\Omega$ is independent of energy. $sd\sigma/d\Omega$ for $e^+e^- \to e^+e^-$ measured[9] by the MARK J group at various energies are plotted as a function of scattering angle in Fig. 3. The results for $e^+e^- \to e^+e^-$ and $e^+e^- \to \gamma\gamma$ measured[7] by the JADE Collaboration are shown in Fig. 4. Both experiments are in agreement with the QED prediction represented by the solid line in Figs. 3 and 4. To quantify the agreement it is assumed that a breakdown of QED in $e^+e^- \to e^+e^-$ can be parametrized by introducing spacelike and timelike form factors $F_s(q^2)$ and $F_T(q^2)$. With $F_s(q^2) = F_T(q^2) = 1 \pm \frac{q^2}{q^2 - \Lambda_\pm^2}$ the agreement with QED can be expressed as a lower limit on the cut off parameter $\Lambda_\pm$.

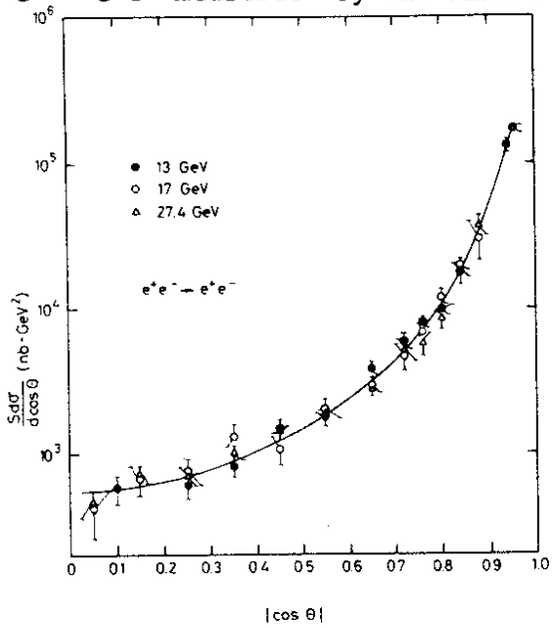

Fig. 3 - The cross section $s \cdot \frac{d\sigma}{d\Omega}$ for $e^+e^- \to e^+e^-$ measured by MARK J between 13 and 27.4 GeV in c.m.

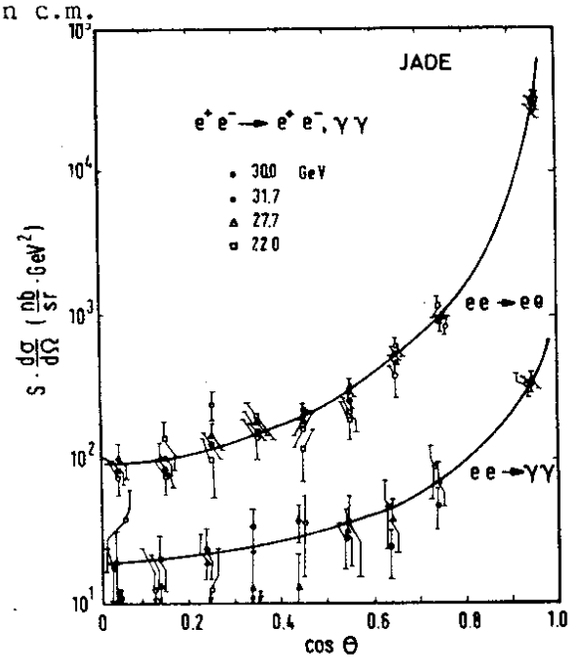

Fig. 4 - The cross section $s \cdot \frac{d\sigma}{d\Omega}$ for $e^+e^- \to e^+e^-$ and $e^+e^- \to \gamma\gamma$ measured by JADE between 22 and 31.7 GeV in c.m.

The results are listed in Table II.

Table II - Lower limits on $\Lambda_\pm$ at 95% confidence in $e^+e^- \to e^+e^-$

	Λ_+(GeV)	Λ_-(GeV)
MARK J[9]	65	64
JADE[7]	89	74
PLUTO[10]	71	67

A possible breakdown of QCD in $e^+e^- \to \gamma\gamma$ can be expressed as

$$d\sigma/d\Omega = (1 \pm \frac{s^2}{2\Lambda_\pm^4} \sin^2\theta) \left(\frac{d\sigma}{d\Omega}\right)_{QED} \qquad (2)$$

From a fit to the data the JADE Collaboration finds[17] $\Lambda_+ > 43$ GeV and $\Lambda_- > 31$ GeV with 95% confidence.

Fig. 5 shows the total cross section for $e^+e^- \to \mu^+\mu^-$ and $e^+e^- \to \tau^+\tau^-$ as reported[9] by the MARK J group. The solid(dashed) line is the QED prediction for pointlike leptons. The agreement is good and to express the agreement in terms of a radius of the leptons

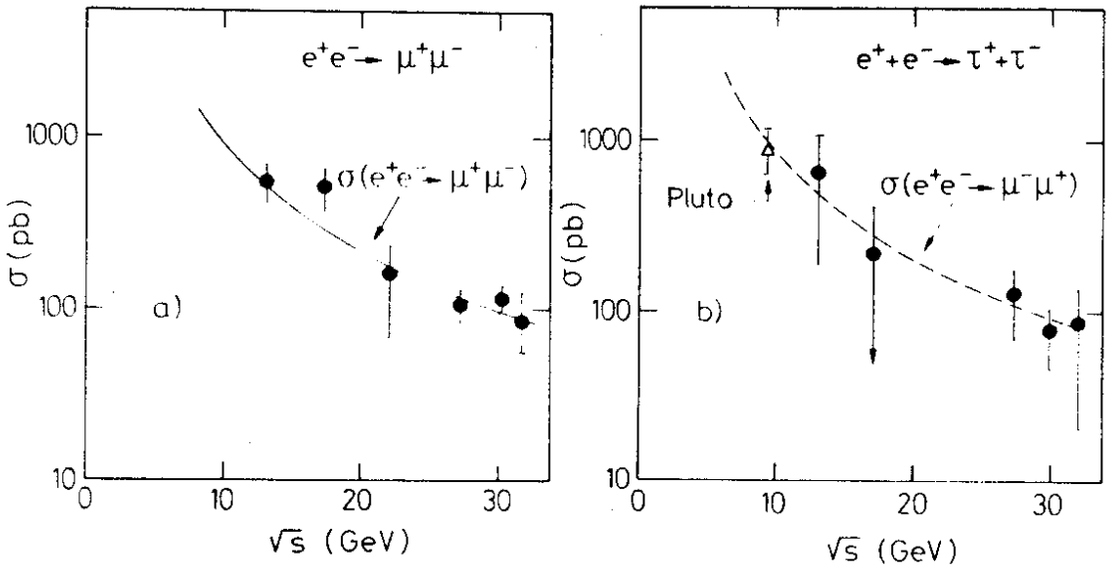

Fig. 5 - The total cross section for $e^+e^- \to \mu^+\mu^-$ and $e^+e^- \to \tau^+\tau^-$ measured by MARK J

the MARK J group assumes a form factor:

$$F_\ell(q^2) = 1 \mp \frac{q^2}{q^2 - \Lambda^2_{\ell\pm}} \qquad (3)$$

A fit to the data give:

ℓ	electron	muon	tau
Λ_-	95 GeV	97 GeV	53 GeV
Λ_+	74 GeV	71 GeV	97 GeV

Lepton universality is thus valid down to distances of 10^{-16} cm.

In models incorporating several neutral vector bosons, the lightest vector boson always has a mass below the mass given in the standard[11] Weinberg-Salam model. Therefore, although they can be made to yield the same prediction as the standard model at low energies, they will differ at high energies. JADE[7] has fitted their data to a particular version[12] of such a model with the mass M, and the width Γ_1 of the lightest neutral vector boson as a parameter. The result is shown in Fig. 6.

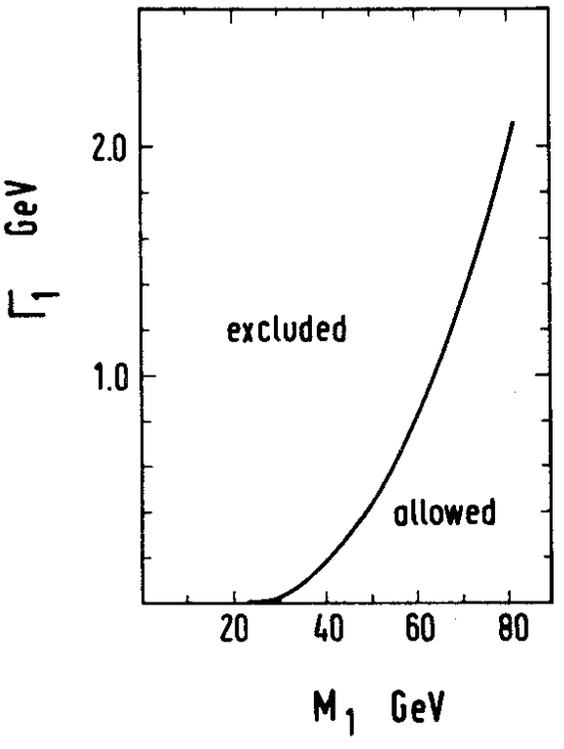

Fig. 6
Limits on the width and mass at the lightest neutral vector boson in a two pole model. The data are from JADE.

3. HADRON PRODUCTION IN e^+e^- ANNIHILATION

It has been conjectured[13-16] that hadron production in e^+e^- annihilation proceeds by quark pairproduction as shown in Fig. 7a, where the electromagnetic current couples directly to the charge of a pointlike quark. (The neutral weak current is expected to contribute on the order of 1% to the total cross section at PETRA energies and is neglected). The total cross section for hadron production is therefore proportional to the cross section for muon pairproduction with the constant of proportionality

$$R = \frac{(e^+e^- \to \text{hadrons})}{(e^+e^- \to \mu^+\mu^-)} = 3 \sum_i \left(\frac{e_i}{e}\right)^2 \qquad (4)$$

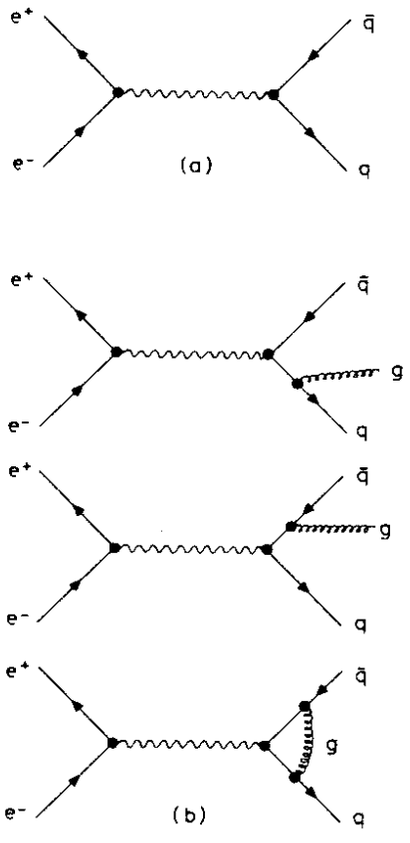

Fig. 7 - Quark pairproduction and gluon bremsstrahlung to first order

Here e_i is the charge of the i-th flavour and the sum is over all flavours. The hadrons will appear in two nearly collinear jets of hadrons with small and maybe constant momenta transverse and large and growing momenta parallel to the jet axis. The single particle distribution should scale i.e.

$s \cdot \frac{d\sigma}{dx}$ with $x = E_h/E_{beam}$ should be independent of energy for large x. The charged particle multiplicity is expected to increase logarithmically with $s = (2E)^2$. The data[17] from SPEAR and DORIS at lower energies support the gross features of this picture.

This picture will be modified in any field theory[18] of strong interactions. In a field theory e^+e^--annihilation proceeds to lowest order by the Feynman graphs shown in Fig. 7b. The produced quark radiate field quanta (gluons) and the gluons are expected to materialize as hadron jets in the final state.

This has well defined experimental implications[19,20]: The mean transverse momentum of the hadrons with respect to the jet axis will increase with energy. If the quark-gluon coupling constant is small only one of the jets will broaden. The premordial $q\bar{q}g$ state is necessarily planar and the final hadron configuration will retain the planarity. In a small fraction of the events the gluon is radiated at an angle which is large compared to the angular spread of the hadron jet. Such events will be very striking with three visible jets of hadrons defining a plane.

A field theory of the strong interactions will also modify the value for R given above, the multiplicity will grow faster than ln s and the single particle distribution will no longer scale.

At present quantum chromodynamics (QCD)[21] is the leading candidate for a theory of strong interactions. The coupling constant in this theory depends on $q^2 = (2E)^2$ and is given by

$$\alpha_s(q^2) = g^2/4\pi = \frac{12\pi}{(33-2N_f)\ \ln\ q^2/\Lambda^2} \quad . \qquad (5)$$

Here N_f is the number of flavours with mass below E and Λ is determined[22] in deep inelastic lepton-hadron interactions to be about 500 MeV. The data will be confronted with the QCD predictions. However it is important to bear in mind that most of the general features outlined above will be true in any field theory of strong interactions.

3.1 THE TOTAL CROSS SECTION

In some respects a measurement of the total hadronic e^+e^- annihilation cross section is easier at high than at low energies. The final state hadrons are in general confined in two back to back jets and the angular distribution of the jet axis is proportional to $1 + \cos^2\theta$. The new generation of detectors cover a large solid angle and this, together with the high multiplicity, result in a high detection efficiency (75-80%) which is subject to small systematic uncertainties only. Events resulting from cosmic radiation or from interactions between the beam and the environment are easily identified and removed in the off line analysis. The background from $e^+e^- \to \tau\bar{\tau}$ lead to events with low multiplicity (90% of all $\tau\bar{\tau}$ lead to events yield 4 or less prongs) and are removed by a cut on multiplicity. The contribution from two photon processes $e^+e^- \to e^+e^-$ hadrons are removed by a cut on visible energy.

The values[2,9,23-25] for R at PETRA energies, corrected for radiative effects and with the contribution from $e^+e^- \to \tau^+\tau^-$ removed, are plotted in Fig. 8 together with data[26] measured at lower energies. In addition to the statistical errors shown, there is a systematic uncertainty on the order of 10%. The different groups collected data using different trigger conditions and they applied different cuts to extract the R values. The good agreement among the various groups demonstrate that systematic effects are well understood.

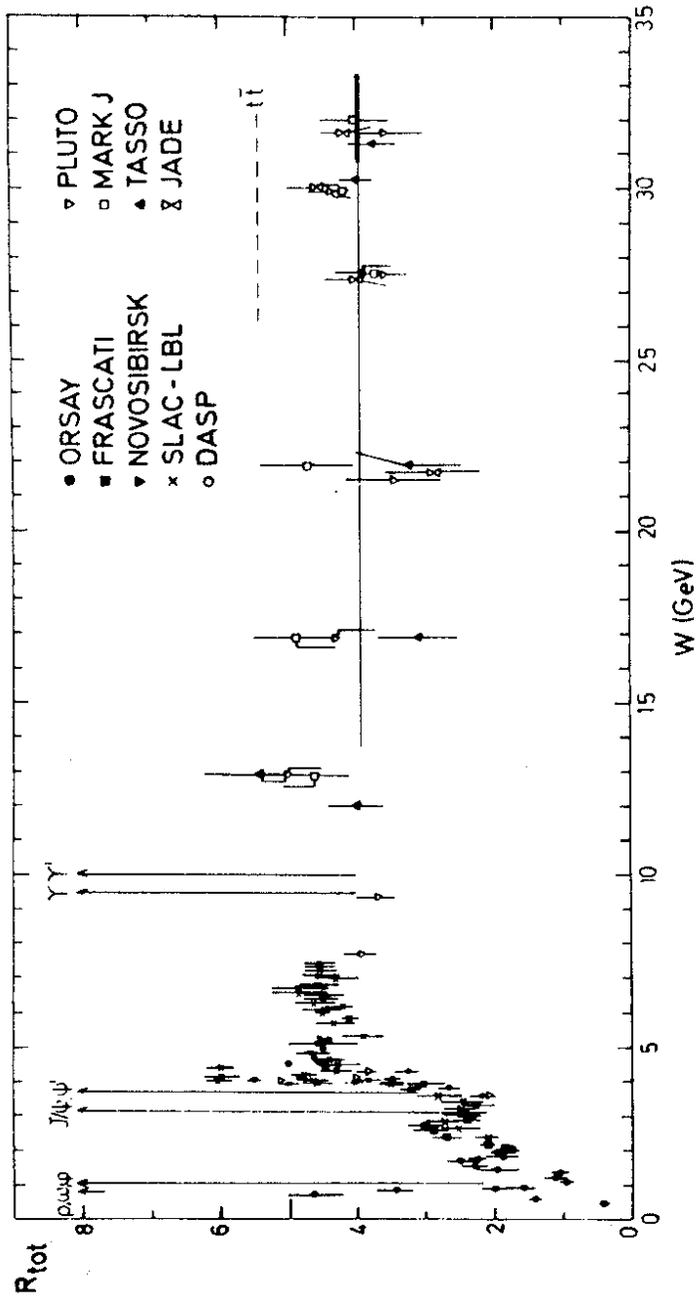

Fig. 8 - R as a function of c.m. energy. The solid line is the QCD prediction for u, d, s, c and b quarks

The new data finds R to be constant above 13 GeV in c.m. In the parton model with u, d, s, c and b quarks R = 3.7. First order QCD predict[27] $R = (1 + \alpha_s(q^2)/\pi)\ 3 \cdot \Sigma(e_i/e)^2$, i.e. a small increase of about 6% only. This prediction, shown as the solid line in Fig. 8, is in good agreement with the data. If we naivly average the R values for all experiments above 27 GeV in c.m. and ignore

systematic uncertainties we find <R> = 3.94 compared to the QCD value of 3.92. Of course the data are not yet accurate enough, once systematic errors are included, to discriminate between the quark-parton and the QCD predictions for R.

A charge 2/3 e quark would lead to R ≈ 5.4, shown as the dotted line in Fig. 8, in disagreement with the observed R values. However, the data are not yet precise enough to exclude a charge 1/3 e quark. There is also no evidence in the data for pairproduction of new leptons. However, note that new leptons will yield final states with a lower multiplicity than those observed in multihadron states and hence have a lower trigger efficiency.

3.2 CHARGED MULTIPLICITY AND RAPIDITY DISTRIBUTIONS

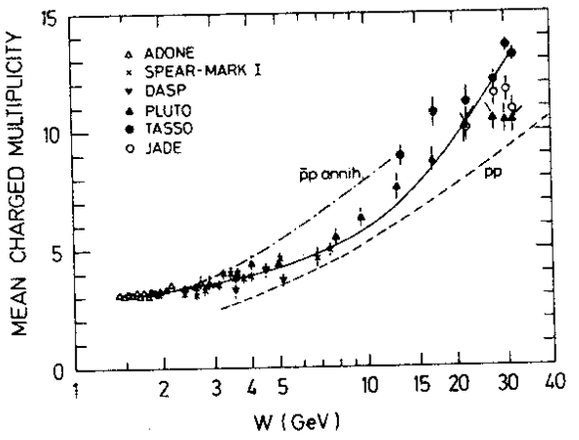

Fig. 9 - Average charged particles multiplicity versus the c.m. energy. The solid line is a combined fit to the low energy data and the TASSO data at high energies

The average charged multiplicity observed[10,24,28] at high energies $\langle n_{ch} \rangle$ is plotted in Fig. 9 together with data[29] at lower energies as a function of W (W = 2E). For comparison the multiplicities observed in pp[30] and $p\bar{p}$[31] collisions are shown as the dashed and the dashed-dotted line in Fig. 10. The data are clearly not proportional to a + b ln s over the whole energy range, as predicted in the naive quark-parton model. Indeed a fit to the data for 1.4 GeV < W < 7 GeV yield a = 2.67 ± 0.04 and b = 0.48 ∓ 0.02. At W = 30 GeV this fit predicts a charged multiplicity of 6 compared to an observed multiplicity of more then 10. Pair production of bottom quarks is expected to increase the multiplicity by 0.2 and cannot account for the strong increase.

The multiplicity in QCD is expected[32] to behave as $\langle n_{ch} \rangle = n_o + a \exp(b \sqrt{\ln s / \Lambda^2})$. A fit to the data[28] for 1.4 GeV < W < 31.5 GeV yields:

$$\langle n_{ch} \rangle = (2.92 \pm 0.04) + (0.0029 \pm 0.005) \exp(2.85 \pm 0.07)(\ln s/\Lambda^2)^{1/2}$$

and is shown as the solid line in Fig. 9. The general trend of the data is reproduced by the fit.

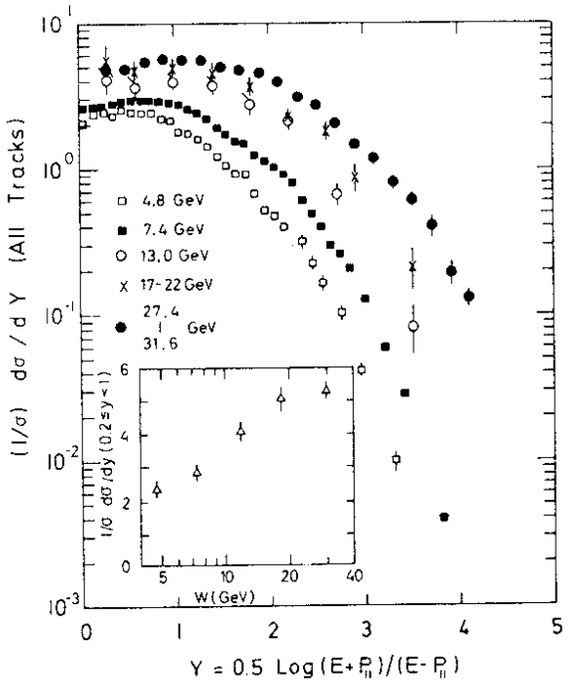

Fig. 10
Rapidity distributions for charged particles assuming they are pions. The data at 4.8 GeV and 7.4 GeV are from SLAC-LBL. The high energy data are from TASSO

The rapidity distribution of charged particles, evaluated with respect to the jet axis and normalized to the total cross section, is plotted in Fig. 10. The jet axis was determined using thrust (see below). The rapidity $Y = 0.5 \ln (E+p_{//})/(E-p_{//})$ where E is the energy and $p_{//}$ the momentum of the particle with respect to the jet axis, was evaluated assuming the particles to be pions. The high energy data were obtained by the TASSO Collaboration[28] and they are compared with data from the SLAC-LBL Collaboration[29] at 4.8 and 7.4 GeV. The distribution has a clear plateau at Y = 0 and this plateau becomes longer with increasing energy. The height of the plateau, however, is not constant as expected in quark-parton models, but also increases with energy. This is shown clearly in the insert to Fig. 10, where the normalized cross section $1/\sigma \, d\sigma/dy$ for $0.2 \leq Y < 1.0$ is found to increase linearely with ln W.

To compare the fragmentation regions at various energies the data are replotted in Fig. 11 versus $Y-Y_{max}$ where $Y_{max} \approx 0.5 \ln(s/m^2)$.

The width and the shape of the fragmentation region are nearly independent of energy with the high energy data slightly below the data obtained at lower energies. This is in qualitative agreement with scaling violations expected to occur in QCD. However, it is important to note that the intrinsic resolution is about 1 unit in rapidity caused by the uncertainty in determining the jet direction.

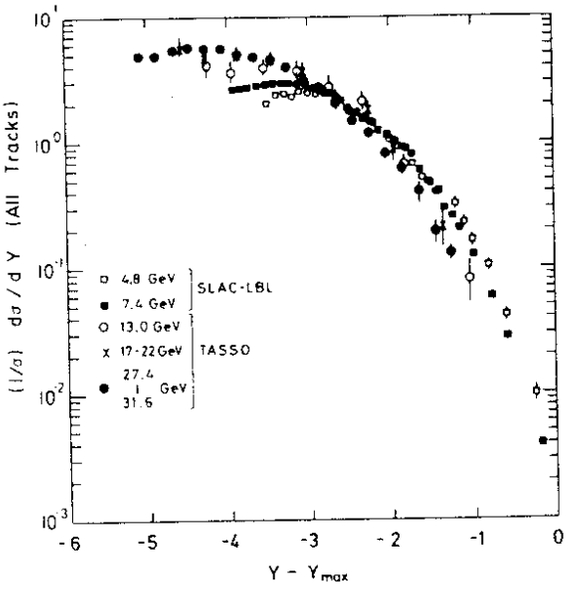

Fig. 11 – The same data as in Fig. 10 plotted versus $Y-Y_{max}$

The rise of the plateau with energy and the near energy independence of the distributions in the fragmentation region shows that the rise in multiplicity is caused by an excess of low energy particles

3.3 SCALING

The cross section $sd\sigma/dx$ with $x = p/p_{beam}$ can be expressed at high energies ($\beta \gtrsim 1$) in terms of two scaling functions $\bar{W}_1$ and $\bar{W}_2$

$$s\frac{d\sigma}{dx} = 4\pi\alpha^2 \cdot x\left(m\bar{W}_1 + \frac{1}{6}s\nu\bar{W}_2\right) \qquad (6)$$

Here $\nu = \sqrt{s} \cdot E/m$ is the photon energy seen in the rest system of the particles.

Data from DASP[29] at 5 GeV, from SLAC-LBL[33] at 7.4 GeV and from TASSO[28] for energies between 13 and 31.6 GeV are plotted in Fig. 12 The cross sections for $x > 0.2$ scale to within 30% between 5 GeV and 31.6 GeV. For $x < 0.2$ the cross section shows a dramatic rise with energy between 5 GeV and 30 GeV. This rise is related to the strong growth of the multiplicity discussed above.

Gluon emission as indicated in Fig. 7b will lead to a depletion of particles at large x and a corresponding increase in the yield at small x, since the energy is now shared between the quark and the gluon. In QCD, however, these effects are only on the level of 20% since the Q^2 values are large compared to the scale breaking parameter $\Lambda^2 = 0.25\ GeV^2$.

More precisely[34] the 30 GeV data for $x = 0.2$ are predicted to be higher by 10% and for $x = 0.7$ lower by $\sim$ 20% in comparison with the 5 GeV data. The present data are not precise enough to test this prediction.

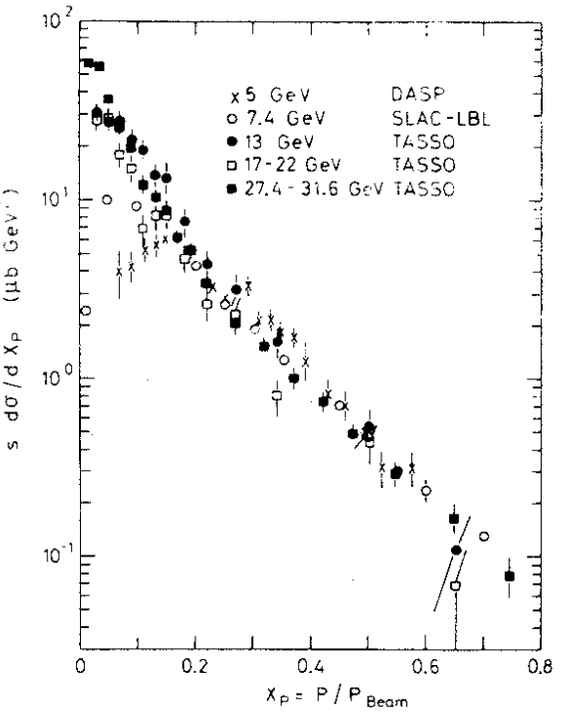

Fig. 12
The scaling cross section s dσ/dx ($x = p/p_{beam}$) for inclusive charged particle production

4. EVIDENCE FOR GLUONS AND AGAINST NEW FLAVOURS

The topology of the hadrons in e^+e^- annihilation can be used to identify the production mechanismn:

a) Pairproduction of light quarks manifests itself as two back to back narrow jets of hadrons
b) pairproduction of heavy quarks will, close to threshold, lead to nearly spherical events
c) Gluon bremsstrahlung $e^+e^- \rightarrow q\bar{q}g$ leads to planar events with large momenta in the plane and small momenta with respect to the plane. A fraction of the events will have a clear three-jet structure.

All groups have made extensive Monte Carlo computations to confront various production mechanismns with the data. The computations are in general based on the formalismn developed by Feynman and Fields[35]. In their model the various quark flavours are pairproduced proportional to e_f^2. Light quarks pairs are created in vacuum in the ratio: uu : dd : ss = 2 : 2 : 1. The quarks fragments according to the distribution function $f(z) = 1-a+3a\,(1-z)^2$ with $a = 0.77$ and $z = E_{meson}/E_{quark}$. A flat distribution function is also used for heavier quarks. The primary mesons are created with a Gaußian distribution $\exp(-p_T^2/2\sigma_q^2)$ around the jet axis. From fits to deep inelastic lepton-hadron data σ_q was found[35] to be about 250 MeV/c. The decay modes for light primary mesons are taken from the particle data tables. Decay mode for heavier mesons were estimated[36] using various models. The fragmentation for the gluon is discussed in the paper by Hoyer et al.[20].

4.1 THRUST AND SPHERICITY DISTRIBUTIONS

Two methods to determine the jet axis, sphericity[15] and thrust[37,38] are in general use:

$$\text{Sphericity S is defined as } S = \frac{3}{2} \min \frac{\Sigma_i (p_T^i)^2}{\Sigma_i (p^i)^2} \qquad (7)$$

Here p^i is the momentum and p_T^i the transverse momentum of a track with respect to a given axis. The jet axis is defined as the axis which minimizes transverse momentum squared. Sphericity measures the square of δ, the jet cone opening angle. $S = 3/2 \langle\delta^2\rangle$ and is 0 for a perfect jet and 1 for a spherical event.

$$\text{Thrust T is defined as } T = \max \frac{\Sigma_i |p^i|}{\Sigma_i |p^i|}$$

Here p^i is the momentum of a track and $p_{//}^i$ its projection along a given axis. The jet axis is defined as the axis which maximizes the directed momentum. Expressed in terms of δ, $T \approx (1-\langle\delta\rangle^2)^{1/2}$ and it will approach 1 for a perfect jet event and 1/2 for an isotropic event.

The deviation between the true jet axis and the axis found by either the sphericity or the thrust method was determined by a Monte Carlo computation. The result is plotted in Fig.13 as a function of energy. The jet axis is determined to 5° or better nearly independent of method for c.m. energies above 20 GeV.

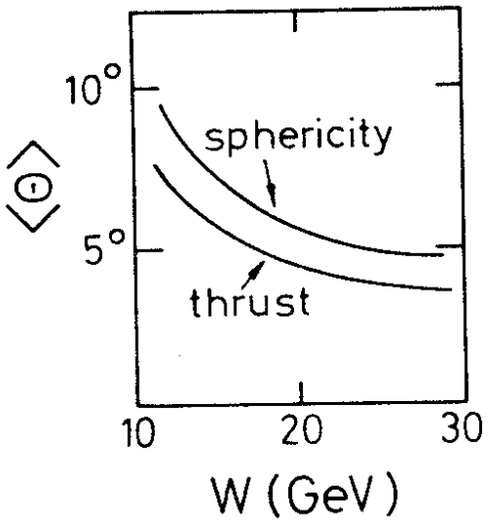

Fig. 13
A Monte Carlo calculation of the angular deviation between the true jet axis and the axis determined using either sphericity or thrust

The sphericity distribution 1/N(dN/dS) as measured by TASSO[25] and the differential thrust distribution as measured by PLUTO[23] are shown in Fig. 14 and Fig. 15 respectively. The jets are expected to become more collimated with increasing energy and this trend is clearly observed in the data. The solid line shows the $q\bar{q}$ prediction including u, d, s, c and b quarks. The TASSO Monte Carlo also in-

cludes gluon bremsstrahung.

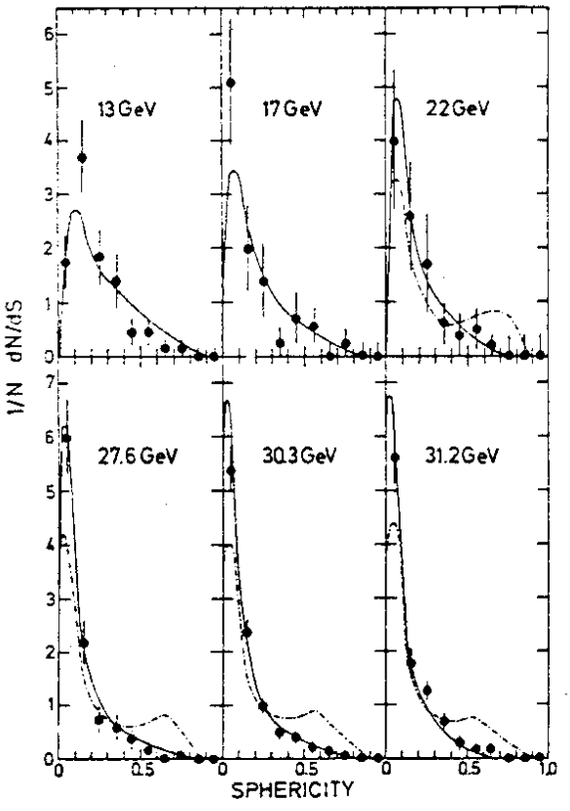

Fig. 14
Sphericity distributions for different c.m. energies measured by the TASSO Collaboration. The curves show the prediction for u, d, s, c and b quarks (solid) plus t quark contribution (dashed-dotted) curves

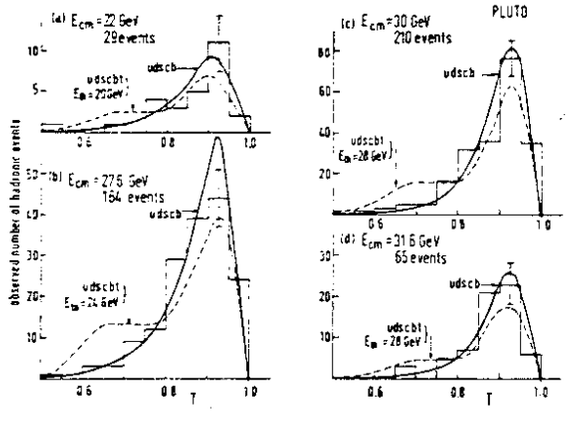

Fig. 15
Thrust distributions for various c.m. energies measured by the PLUTO Collaboration. The curves show the prediction for u, d, s, c and b quarks (solid) plus t quark (dotted)

A) GROWTH OF TRANSVERSE MOMENTUM WITH ENERGY

The naive quark-parton model assumes that the transverse momentum of the hadrons with respect to the jet axis remains constant independent of energy. In QCD the transverse momentum squared will grow proportional to Q^2 i.e. effects from QCD will become increasingly prominent with energy.

The normalized transverse momentum distribution $(1/\sigma)d\sigma/dp_T^2$ measured[4] by TASSO and evaluated with respect to the sphericity axis is plotted in Fig. 18 versus p_T^2. The data at 13 GeV and 17 GeV are identical within statistics and are averaged, similarly

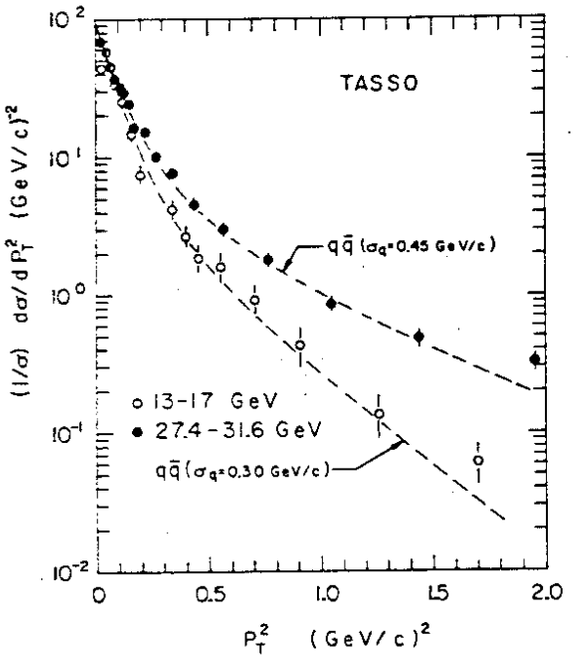

Fig. 18
$1/\sigma\ d\sigma/dp_T^2$ at 13 and 17 GeV combined and for c.m. energies between 27.4 and 31.6 GeV combined as a function of p_T^2. The curves are $q\bar{q}$ fits to the data for $p_T^2 < 1.0$ $(GeV/c)^2$ including u, d, s, c and b quarks with σ_q as a free parameter

the data between 27.4 and 31.6 GeV are combined. The data at both energies are in resonable agreement for $p_T^2 < 0.2$ $(GeV/c)^2$ but the high energy data are well above the low energy data for large values of p_T^2 - i.e. the average p_T^2 is clearly increasing with energy. The data at 13 - 17 GeV have been fit to $e^+e^- \to q\bar{q}$ for $p_T^2 < 1.0$ $(GeV/c)^2$ with $<\sigma_q>$ as a variable. The results, shown as the dashed line in Fig. 18, yield $<\sigma_q> = 300$ MeV/c compared to $<\sigma_q> \sim 250$ MeV/c extracted from deep inelastic lepton hadron data. To fit the higher energy data $<\sigma_q>$ must be increased to 450 MeV/c. A good fit to the high energy data can also be obtained by using $<\sigma_q> = 300$ MeV/c and including gluon bremsstrahlung. Hence the p_T^2 distribution alone cannot be used to discriminate between the $q\bar{q}$ model with an energy dependent value of σ_q and the $q\bar{q}g$ model with a constant value for σ_q.

C) PLANARITY OF THE EVENTS

Regardless of the value of $\langle p_T \rangle$ hadrons resulting from the fragmentation of a quark must on the average be uniformly distributed in azimuthal angle around the quark axis. Therefore, apart from statistical fluctuations, the two-jet process $e^+e^- \to q\bar{q}$ will not lead to planar events whereas the radiation of a hard gluon, $e^+e^- \to q\bar{q}g$, will result in an approximately planar configuration of hadrons with large transverse momenta in the plane and small transverse momenta with respect to the plane. Thus the observation of such planar events at a rate significantly above the rate expected from statistical fluctuations of the $q\bar{q}$ jets shows in a model independent way that there must be a third particle in the final state which might be identified with a gluon.

The shape of an event is conviniently evaluated by constructing the second rank tensor[15,17]

$$M_{\alpha\beta} = \sum_{j=1} p_{j\alpha} \cdot p_{j\beta} \qquad (\alpha,\beta = x,y,z) \qquad (9)$$

where $p_{j\alpha}$ and $p_{j\beta}$ are momentum components along the α and β axis for the jth particle in the event. The sum is over all charged particles in the event. Let $\vec{n}_1$, $\vec{n}_2$ $\vec{n}_3$ be the unit eigenvectors of this tensor associated with the normalized eigenvalues Q_i, $Q_i = \Sigma_j(\vec{p}_j \cdot \vec{n}_i)^2 / \Sigma_j p_j^2$, which are ordered such that $Q_1 \leq Q_2 \leq Q_3$. Note that $Q_1 + Q_2 + Q_3 = 1$. The principal jet axis is then $\vec{n}_3$ direction, the event plane is spanned by $\vec{n}_2$ and $\vec{n}_3$; and $\vec{n}_1$ defines the direction in which the sum of the square of the momentum components is minimized.

We first compare the distribution of $\langle p_T^2 \rangle_{out}$, the momentum component normal to the event plane squared, with that of $\langle p_T^2 \rangle_{in}$, the momentum component in the event plane perpendicular to the jet axis.

The data on the $\langle p_T^2 \rangle_{in}$ and $\langle p_T^2 \rangle_{out}$ distribution at low and high energies obtained by TASSO[4] and JADE[7] are plotted in Figs. 22-24. All groups observe that $\langle p_T^2 \rangle_{out}$ changes little with energy in contrast to the distribution of $\langle p_T^2 \rangle_{in}$ which grows rapidly with energy, in particular there is a long tail of events not observed at lower energies. The $\langle p_T^2 \rangle_{out}$ distributions at both low and high energies are described reasonably well with $e^+e^- \to q\bar{q}$ - i.e. the momenta transverse to the event plane is consistent with the quarks fragmenting into hadrons with a constant transverse momentum independent of energy. The same model also describes the $\langle p_T^2 \rangle_{in}$ distribution at low energies, but it completely fail to reproduce the long tail observed in $\langle p_T^2 \rangle_{in}$ at high energies. This discrepancy cannot be removed by increasing the mean transverse momentum of the jet. Fig. 22 shows a fit assuming σ_q = 450 MeV/c (which gave a good fit to $1/\sigma\, d\sigma/dp_T^2$). The agreement is poor. We therefore conclude that the data include a number of planar events not reproduced by the $q\bar{q}$ model independent of the average p_T assumed. However, as shown in Figs. 23 and 24 the long tail of the $\langle p_T^2 \rangle_{in}$ distribution can be accounted for in the qqg model.

In Fig. 19 $\langle p_T^2 \rangle$ measured by PLUTO and TASSO is plotted versus c.m. energy. These data have not been corrected for detector acceptances. Both groups find that $\langle p_T^2 \rangle$ is increasing with energy in agreement with a QCD calculation done by Hoyer et al[20]. A $q\bar{q}$ model with constant σ_q is excluded, however, a good fit can also be obtained in this model if σ_q is allowed to vary. This is not excluded on general grounds.

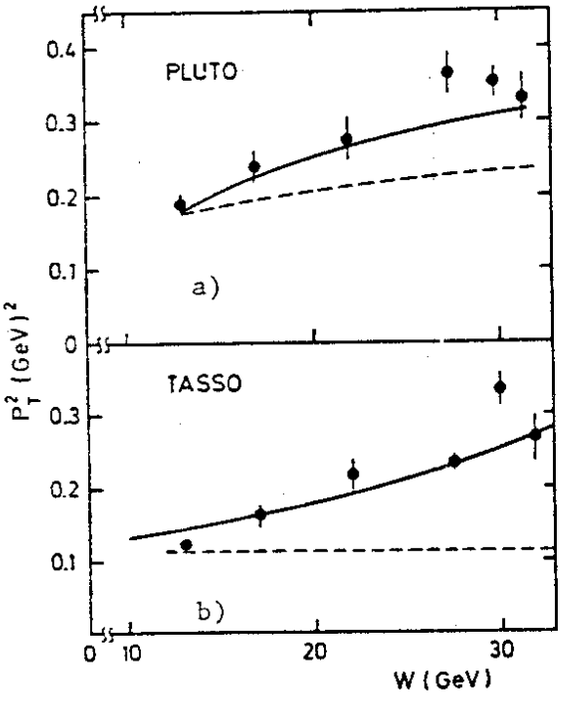

Fig. 19
a) The observed transverse momentum squared of charged particles with respect to the jet axis defined by thrust. The data were obtained by PLUTO. They are not corrected for acceptance. The solid line is the prediction for $e^+e^- \to q\bar{q}$ with constant σ_q. The solid line is a QCD prediction by Hoyer et al.[20]
b) Same as in a) except the data were obtained by TASSO

B) ONLY ONE JET BROADN

If hard noncollinear gluon emission is a rare process, as expected in QCD, then there should usually be only one gluon per event. In fact the probability of emitting two gluons in one event compared to single gluon emission is proportional to α_s. Only one of the jets should therefore broadn.

To test this prediction the jets in an event are divided into a narrow and a wide jet. In Fig. 20 and Fig. 21 the data obtained by PLUTO[6] and TASSO[4] are shown. Plotted are $\langle p_T^2 \rangle$ versus $z = p/p_{beam}$ at low and high energies for the wide and the narrow jet separately. A large asymmetrie between the two jets is observed by both experiments at high energy. At low energies the observed distributions are more symmetric and they are well reproduced by $e^+e^- \to q\bar{q}$ using the canonical value for $\langle \sigma_q \rangle$. The observed narrow-wide asymmetry is due to statistical fluctuations. The model with constant σ_q fails to describe the data at high energies. Increasing

$\langle\sigma_q\rangle$ to 450 MeV for TASSO and to 350 MeV for PLUTO improves the fit. PLUTO has also computed the distributions for $e^+e^- \to q\bar{q}g$. The agreement with the data is good. Also the TASSO data are reproduced by $e^+e^- \to q\bar{q}g$.

QCD explains naturally the large asymmetry observed in the transverse spread of the two jets in an event. A $q\bar{q}$ model with σ_q increasing with energy results in a worse fit, however such an explanation cannot be completely excluded by the present data.

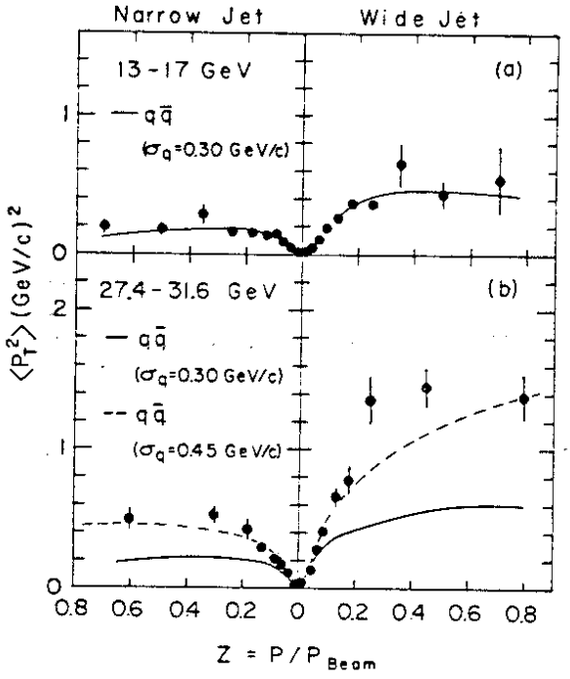

Fig. 20
Data obtained by TASSO on $\langle p_T^2\rangle$ as a function of $Z \equiv p/p_{beam}$ for wide and narrow jets separately, for the low energy (a) and the high energy (b) data. The curves show the prediction from $q\bar{q}$ with σ_T = 0.30 (GeV/c) (solid) and σ_T= 0.45 GeV/c (dotted)

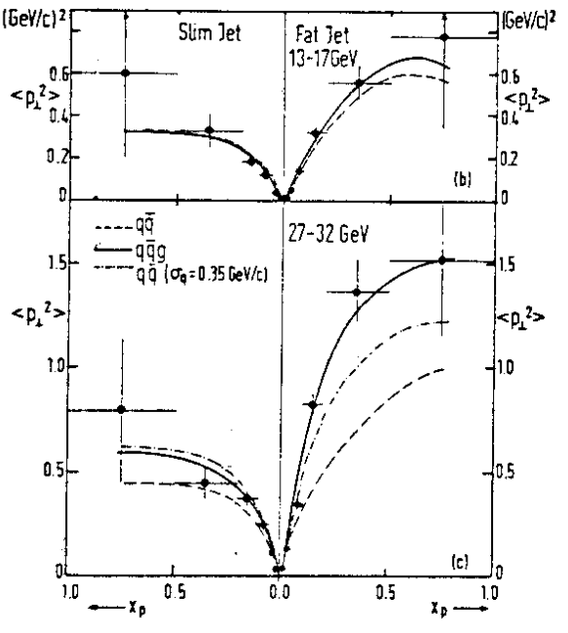

Fig. 21
Data obtained by PLUTO on $\langle p_T^2\rangle$ as a function of $Z = p/p_{beam}$ for wide and narrow jets. The solid and dashed lines are the $q\bar{q}g$ and $q\bar{q}$ predictions, respectively

C) PLANARITY OF THE EVENTS

Regardless of the value of $\langle p_T \rangle$ hadrons resulting from the fragmentation of a quark must on the average be uniformly distributed in azimuthal angle around the quark axis. Therefore, apart from statistical fluctuations, the two-jet process $e^+e^- \to q\bar{q}$ will not lead to planar events whereas the radiation of a hard gluon, $e^+e^- \to q\bar{q}g$, will result in an approximately planar configuration of hadrons with large transverse momenta in the plane and small transverse momenta with respect to the plane. Thus the observation of such planar events at a rate significantly above the rate expected from statistical fluctuations of the $q\bar{q}$ jets shows in a model independent way that there must be a third particle in the final state which might be identified with a gluon.

The shape of an event is conviniently evaluated by constructing the second rank tensor[15,17]

$$M_{\alpha\beta} = \sum_{j=1} p_{j\alpha} \cdot p_{j\beta} \qquad (\alpha,\beta = x,y,z) \qquad (9)$$

where $p_{j\alpha}$ and $p_{j\beta}$ are momentum components along the α and β axis for the jth particle in the event. The sum is over all charged particles in the event. Let $\vec{n}_1$, $\vec{n}_2$ $\vec{n}_3$ be the unit eigenvectors of this tensor associated with the normalized eigenvalues Q_i, $Q_i = \Sigma_j(\vec{p}_j \cdot \vec{n}_i)^2 / \Sigma_j p_j^2$, which are ordered such that $Q_1 \leq Q_2 \leq Q_3$. Note that $Q_1 + Q_2 + Q_3 = 1$. The principal jet axis is then $\vec{n}_3$ direction, the event plane is spanned by $\vec{n}_2$ and $\vec{n}_3$; and $\vec{n}_1$ defines the direction in which the sum of the square of the momentum components is minimized.

We first compare the distribution of $\langle p_T^2 \rangle_{out}$, the momentum component normal to the event plane squared, with that of $\langle p_T^2 \rangle_{in}$, the momentum component in the event plane perpendicular to the jet axis.

The data on the $\langle p_T^2 \rangle_{in}$ and $\langle p_T^2 \rangle_{out}$ distribution at low and high energies obtained by TASSO[4] and JADE[7] are plotted in Figs. 22-24. All groups observe that $\langle p_T^2 \rangle_{out}$ changes little with energy in contrast to the distribution of $\langle p_T^2 \rangle_{in}$ which grows rapidly with energy, in particular there is a long tail of events not observed at lower energies. The $\langle p_T^2 \rangle_{out}$ distributions at both low and high energies are described reasonably well with $e^+e^- \to q\bar{q}$ - i.e. the momenta transverse to the event plane is consistent with the quarks fragmenting into hadrons with a constant transverse momentum independent of energy. The same model also describes the $\langle p_T^2 \rangle_{in}$ distribution at low energies, but it completely fail to reproduce the long tail observed in $\langle p_T^2 \rangle_{in}$ at high energies. This discrepancy cannot be removed by increasing the mean transverse momentum of the jet. Fig. 22 shows a fit assuming $\sigma_q = 450$ MeV/c (which gave a good fit to $1/\sigma\, d\sigma/dp_T^2$). The agreement is poor. We therefore conclude that the data include a number of planar events not reproduced by the $q\bar{q}$ model independent of the average p_T assumed. However, as shown in Figs. 23 and 24 the long tail of the $\langle p_T^2 \rangle_{in}$ distribution can be accounted for in the $q\bar{q}g$ model.

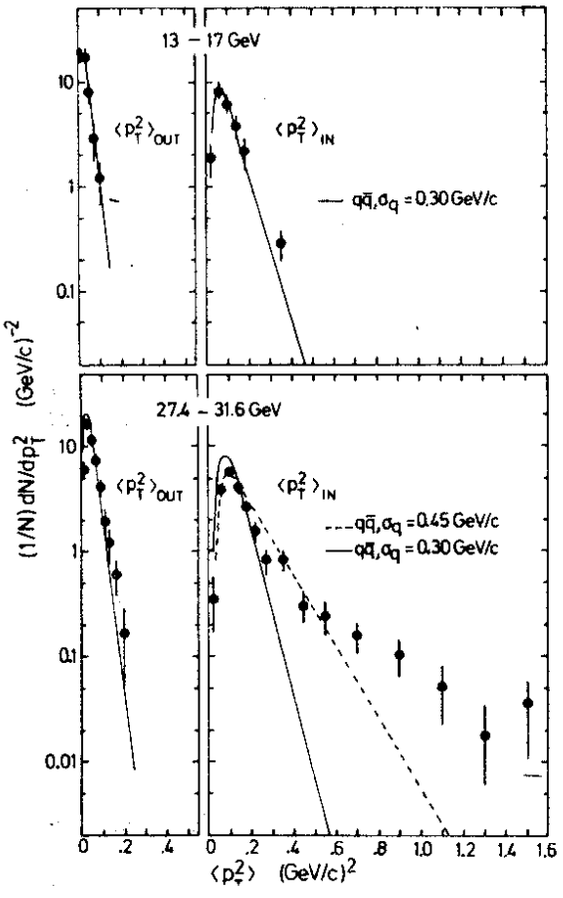

Fig. 22
Distributions of mean transverse momentum squared per event for charged particles, normal to ($\langle p_T^2 \rangle_{out}$) and in ($\langle p_T^2 \rangle_{in}$) the event plane measured by the TASSO Collaboration at low and high energies. The prediction for a $q\bar{q}$ final state with σ_q = 300 MeV/c and σ_q = 450 MeV/c are shown as the solid and the dotted curve respectively

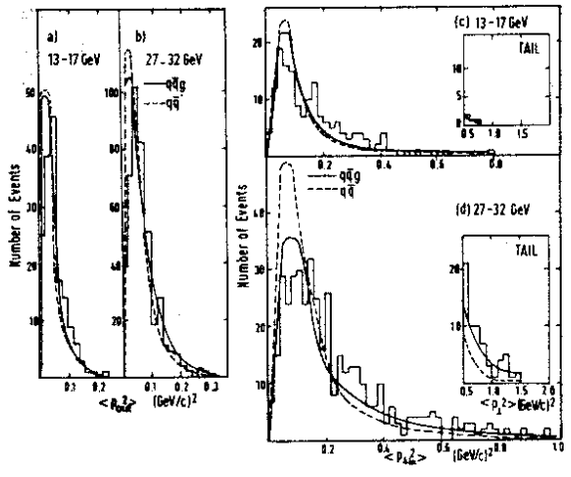

Fig. 23
Similar data as in Fig. 22 obtained by the PLUTO Collaboration. Solid and dashed lines are the $q\bar{q}g$ and $q\bar{q}$ predictions respectively

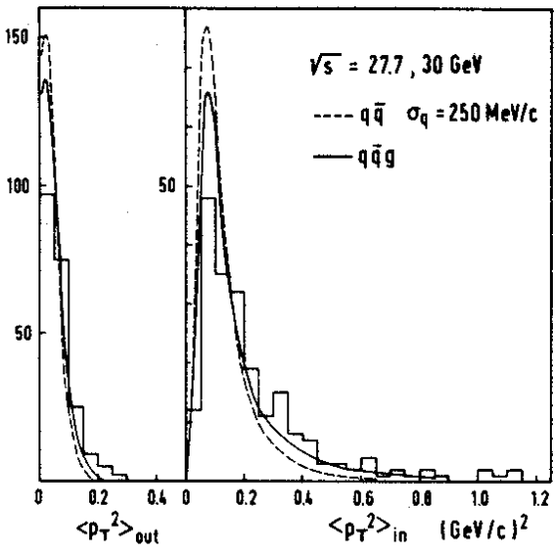

Fig. 24
Similar data as in Figs. 22 and 23 measured by the JADE Collaboration. The dotted and the solid lines are fits to $q\bar{q}$ and qqg respectively

The different energy dependence of $\langle p_T^2\rangle_{in}$ and $\langle p_T^2\rangle_{out}$ is shown strikingly in Fig. 25 using data[4] obtained by TASSO. Each event, viewed along the $\vec{n}_3$ direction, is an ellipsoid with the small and the large axis given by $\langle p_T^2\rangle_{out}$ and $\langle p_T^2\rangle_{in}$ respectively. Fig. 26 shows the computer made overlapp of all these ellipsoids for c.m. energies of 13 GeV, 17 GeV and 27.4 to 31.6 GeV. The slow growth of $\langle p_T^2\rangle_{out}$ and the rapid growth of $\langle p_T^2\rangle_{in}$ with energy are seen rather clearly .

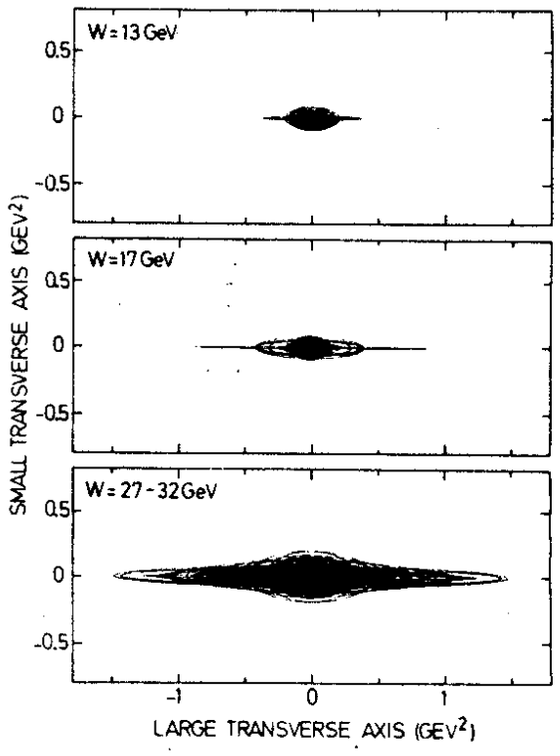

Fig. 25
Events viewed along the jet direction in momentum space. Each event is represented as an ellipsoid with $\langle p_T^2\rangle_{out}$ and $\langle p_T^2\rangle_{in}$ as the minor and major axis. Shown are the sum of all TASSO events at various c.m. energies

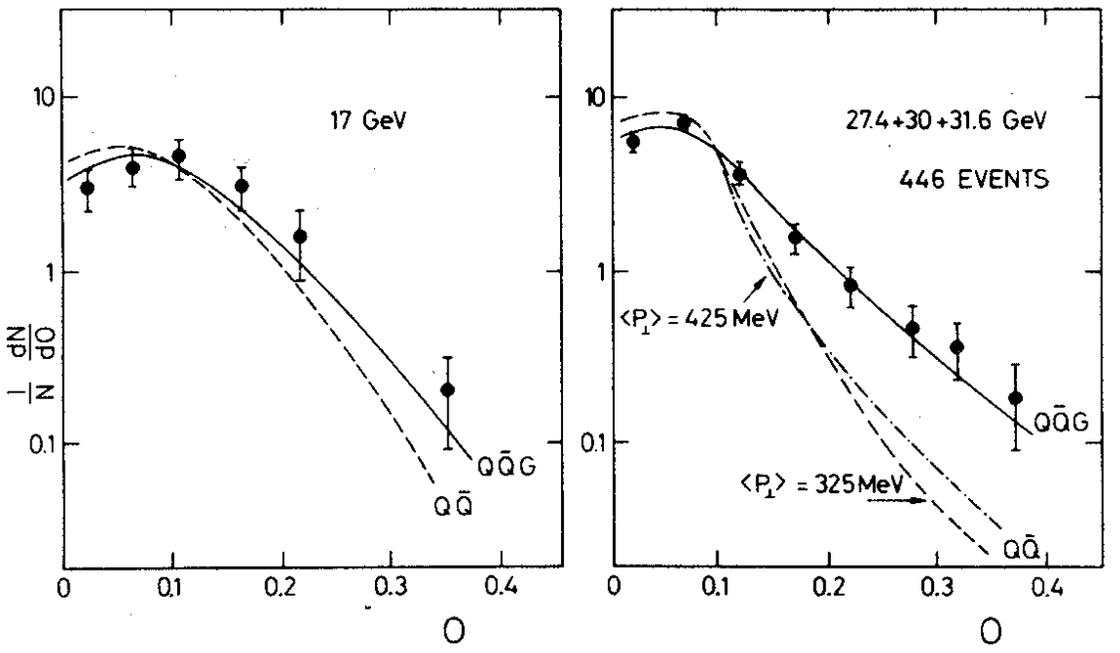

Fig. 26 - The distribution 1/N dN/dO as a function of oblateness for W = 17 GeV and for W between 27.4 GeV and 31.6 GeV. The solid curves are predictions based on $e^+e^- \to qqg$, the dotted curve shows the prediction for $e^+e^- \to q\bar{q}$ with a mean transverse momentum of 325 MeV/c. The dashed-dotted curve is the $q\bar{q}$ model prediction with an average transverse momentum of 425 MeV.

The planarity of the events is also observed[9] by the MARK J group using a different technique. They define a coordinate system as follows: the $\vec{e}_1$ axis coincide with the thrust axis which is defined as the direction of maximum energy flow measured in their segmented calorimeter. They next investigate the energy flow in a plane perpendicular to the thrust axis. The direction of maximum energy flow in that plane defines a direction $\vec{e}_2$ with a normalized energy flow

$$\text{major} = \sum_i |\vec{p}^i \vec{e}_2| \; / \; E_{vis} \qquad (10)$$

where $E_{vis} = \Sigma \vec{p}^i$. The third axis $\vec{e}_3$ is orthogonal to both the thrust and the major axis $\vec{e}_3$, and it is very close to the minimum of the momentum projection along any axis i.e.

$$\text{minor} \sim \sum_i |\vec{p}^i \vec{e}_3| \; / \; E_{vis} \; . \qquad (11)$$

They then define the quantity oblatness O = major-minor as a measure of the planarity. This quantity, apart from statistical fluctuations, will be zero for phase space and two jet events and finite for three jet final states. The normalized event distribution is plotted versus oblatness in Fig. 26 for the 17 GeV data and data between 27.4 GeV and 31.6 GeV separately and compared with predictions for $e^+e^- \to q\bar{q}$ (dashed curve) and $e^+e^- \to qqg$ (solid line).

At 17 GeV acceptable fits are obtained with both models, although the data prefer the fit including gluon bremsstrahlung. At high energies a good fit can be obtained with a $q\bar{q}g$ final state but not with a pure $q\bar{q}$ state, regardless of the value assumed for the average transverse momentum.

The normalized eigenvalues Q_1, Q_2 and Q_3 defined above might be used in a more detailed study of the event shape. The data can be expressed in terms of two variables, aplanarity A and sphericity S

$$A = \frac{3}{2} Q_1 = \frac{3}{2} \frac{\langle p_T^2 \rangle_{out}}{\langle p^2 \rangle} \qquad (12)$$

$$S = \frac{3}{2} (Q_1 + Q_2) = \frac{3}{2} \langle p_T^2 \rangle / \langle p^2 \rangle \qquad (13)$$

All the events are then inside the triangle shown in Fig. 27. Collinear 2 jet events lie in the left hand corner (A, S small), uniform disk shaped events in the upper corner (A small, S large), and spherical events in the lower right hand corner (A, S large), while coplanar events will occupy a band along the larger of the two small sides of the triangle in Fig. 27.

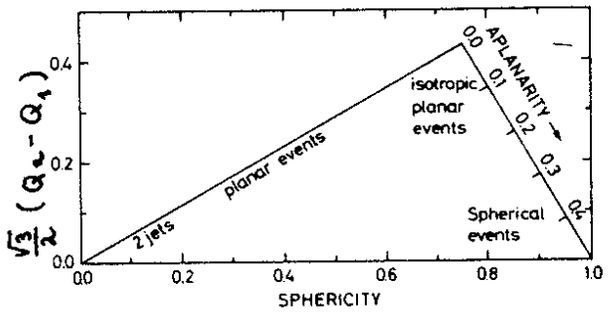

Fig. 27

Distribution of events as a function of aplanarity and sphericity S. Regions in A and S populated by two-jet, planar and spherical events.

The distributions in A and S resulting from:

a) $e^+e^- \to q\bar{q}$ with u, d, s, c and b quarks

b) $e^+e^- \to t\bar{t}$ with m_t = 10 GeV

c) $e^+e^- \to q\bar{q}g$ with q = u, d, s, c and b quarks

are shown in Fig. 28 for a c.m. energy of 30 GeV.

The $q\bar{q}$ model with light quarks indeed populate the region of small A and S with very few events either in the spherical or the planar region.

The $t\bar{t}$ model with m_t = 10 GeV, leads to events with medium values of A and S. Assuming a heavier quark mass will increase values. Note that there are very few planar events in the plot.

The $q\bar{q}g$ model also tends to populate low S and A values but there is a band of planar events resulting from wide angle gluon

radiation.

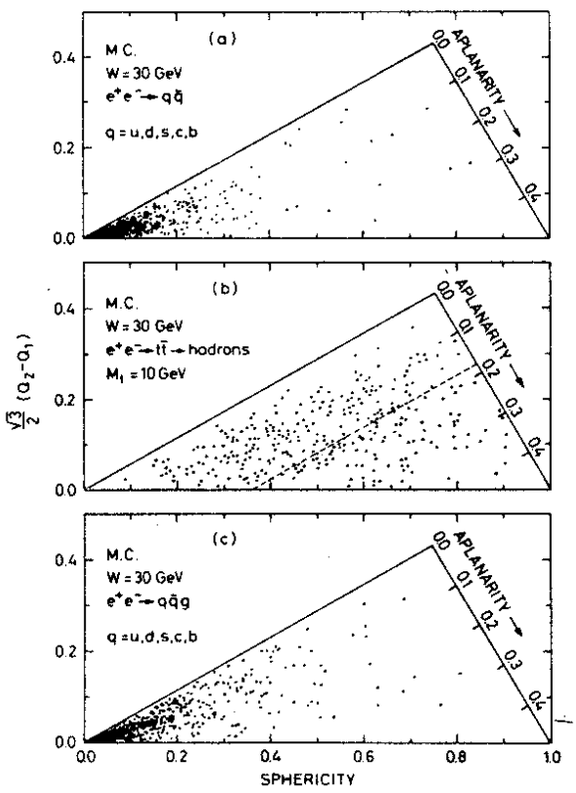

Fig. 28
Monte Carlo created events in aplanarity and sphericity at 30 GeV in c.m. for:

a) $e^+e^- \to q\bar{q}$ with q = u,d,s,c and b quarks

b) $e^+e^- \to t\bar{t}$ with m_t = 10 GeV

c) $e^+e^- \to q\bar{q}g$ with q = u,d,s,c and b quarks

The data obtained by TASSO[25] and JADE[38] are shown in Figs. 29 and 30 respectively.

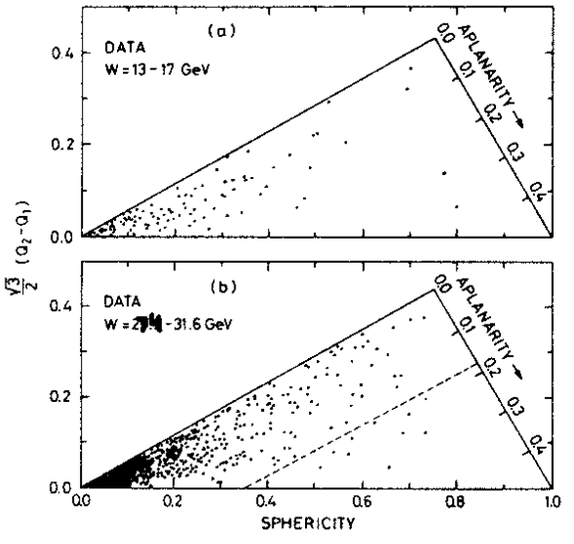

Fig. 29
The event distribution in aplanarity and sphericity observed by the TASSO Collaboration at
a) 13 - 17 GeV
b) at 29.4-31.6 GeV.

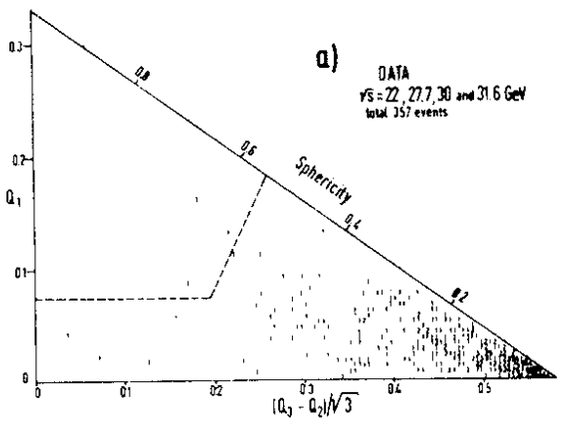

Fig. 30
Similar data as in Fig. 29 obtained by the JADE Collaboration

First, in agreement with the findings discussed above, the data shows no evidence for a heavy quark. Examining the region of large A and S, indicated by the dotted line, both groups put stringent limits on the production of new quarks. These limits are listed in table III and IV.

Table III - The number of events with $S > 0.55$ and $Q_1 < 0.075$ expected in the JADE experiment from production of a quark with charge 2/3 e

Number of events	m_t (GeV)	W (GeV) 22	27.7	30	31.6
expected	8	4	3	2	0
	11		15	22	4
	14			25	5
observed	-	0	1	1	1

Table IV - Limits set by the TASSO-Collaboration on the production of a heavy quark Q with charge 2/3e and 1/3e obtained from the observed number of events with $A > 0.18$

		Number of events				
W(GeV)	observed	predicted qqg	m_Q = 10 GeV 2/3e	1/3e	m_Q = 8 GeV 2/3e	1/3e
29.9-31.6	10	8.2±1.0	80±8	20±2	45±3	11±1
30.9-31.6	2	2.6±0.4	25±1.5	6±0.6	14±1	3.5±0.2

The production of a heavy quark with charge 2/3e in the energy range of PETRA is clearly excluded. The production of a quark with charge 1/3 e seems unlikely.

The production of collinear 2-jet events is seen to dominate at all energies. However, the data at high energy show a band of planar events with small values of A in agreement with a $q\bar{q}g$ final state.

The TASSO data at high energies consist of a total of 949 events (including the data observed during the scan). In a band defined by $A < 0.05$ and $S > 0.25$ there are 62 planar events compared to 49 events predicted by $q\bar{q}g$ and 11 events predicted by $q\bar{q}$.

The JADE Collaboration[38] finds 23 events in band defined by $(Q_3 - Q_2)/\sqrt{3} < 0.35$ and $Q_1 < 0.07$ compared to 22 events predicted for $q\bar{q}g$ and 6 events for $q\bar{q}$.

The PLUTO Collaboration[6] observe 35 events with $S > 0.25$ and $Q_1 < 0.03$. The $q\bar{q}g$ model predict 30 events and the $q\bar{q}$ model 12 events, in the same strip.

The data discussed above proves conclusively that planar events, which cannot result from quark pair production with a Gaußian distribution of transverse momentum around the jet axis are produced in e^+e^- annihilation. Wide angle gluon bremsstrahlung[19] $e^+e^- \to q\bar{q}g$ would naturally result in planar events. The observed rate for such events is consistent with the QCD predictions. Besides this origin, however, there are two ad hoc possibilities; a flat phase space of unknown origin or that the transverse momentum distribution of the quark fragmentation has a long non Gaußian tail. The first possibility can be excluded by observing events with 3 axes, the second by excluding that the 3 axes are not defined by 2 jets and a single high momentum particle at a large angle with respect to the jet axis.

D) PROPERTIES OF PLANAR EVENTS

The PLUTO Collaboration has searched for three-jet events[6] using a generalization[39] of thrust. In this method the final state hadrons with momenta $\vec{p}_1$, $\vec{p}_2$ ... $\vec{p}_N$ are grouped into three classes (Fig. 31a) C_1, C_2 and C_3 with momenta $\vec{P}(C_N) = \Sigma|\vec{p}_i|$ where the sum is over all particles assigned to the class $i \quad C_N$. A new quantity, triplicity T_3, is then defined as

$$T_3 = \frac{1}{\Sigma|\vec{p}_i|} \cdot \text{Max} \; |\vec{P}(C_1)| + |\vec{P}(C_2)| + |\vec{P}(C_3)| \qquad (14)$$

T_3 is 1 for a perfect 3-jet event and $3(\sqrt{3/8}) = 0.65$ for a spherical event. The momenta of the three jets are given by $\vec{P}_1 = \vec{P}(C_1)$, $\vec{P}_2 = \vec{P}(C_2)$ and $\vec{P}_3(C_3)$ (Fig.31b) and the angles between these vectors θ_1, θ_2 and θ_3 are the angles between the three jets. The angles are ordered such that $\theta_1 \leq \theta_2 \leq \theta_3$ and $\theta_1 + \theta_2 + \theta_3 = 360$ since by momentum conservation the three vectors $\vec{P}_1$, $\vec{P}_2$ and $\vec{P}_3$ define a plane. All the events can thus be located in the hatched triangle in Fig. 31b. A totally symmetric 3-jet event ($\theta_1 = \theta_2 = \theta_3 = 120$) would be located in the

corner A. To select the candidates for a three-jet event they make a scatter plot of T_3 versus T (Fig. 31 d). A three-jet event will have large triplicity and small thrust. In the region $T_3 > 0.9$ and $T < 0.8$ they find 48 events at c.m. between 27.4 GeV and 31.6 GeV. With $\sigma_q = 250$ MeV/c a $q\bar{q}$ model predicts 11 events and a $q\bar{q}g$ model 43 events. The angular Dalitz plot for the high energy data is shown in Fig. 31e. The candidates for three-jet events ($T_3 > 0.9$, $T < 0.8$) are shown as large circles, the others as dots. Events with a three jet structure have large values of θ_1; i.e. θ_3 is much less than 180° and θ_1 is large, whereas the black dots representing two jet candidates tend to have small values for θ_1. At high energies they find 52 events with $\theta_1 < 150°$. The $q\bar{q}g$ model predicts 51 and $q\bar{q}$ predicts 19.

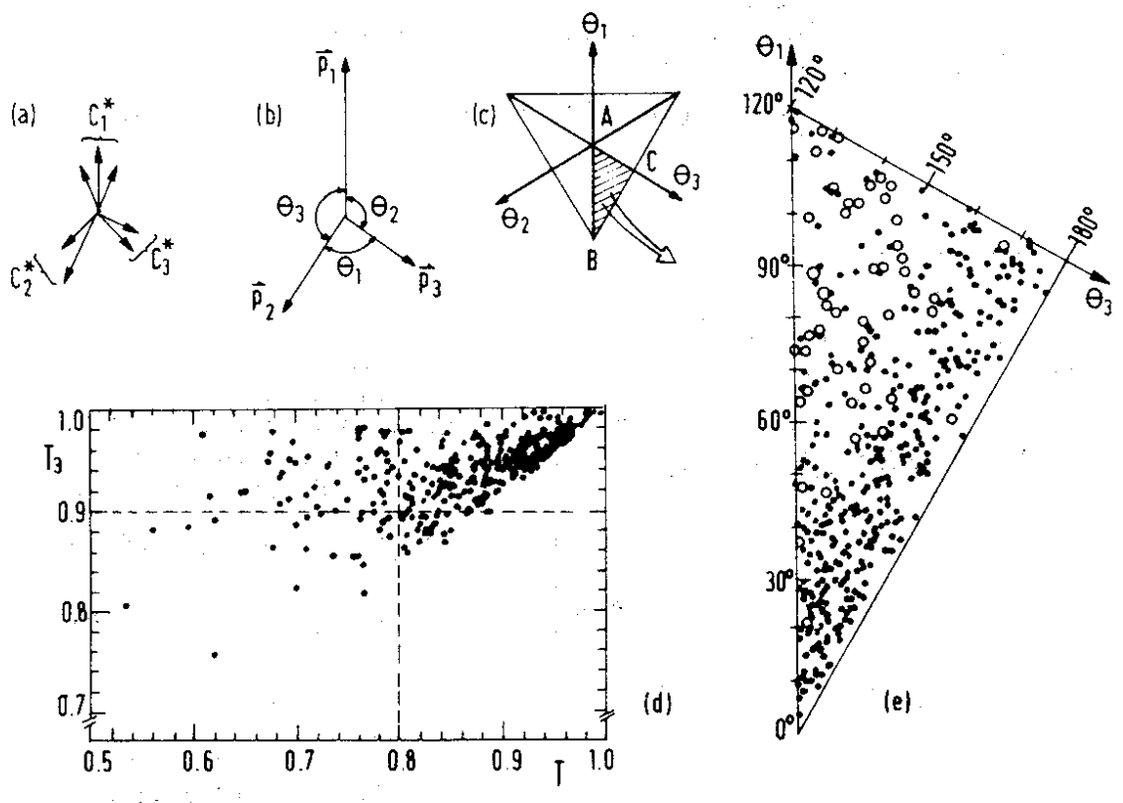

Fig. 31 - a,b) Momentum configuration of hadrons and jets
c) Definition of the angular Dalitz plot with $\theta_3 > \theta_2 > \theta_1$
d) Data obtained by the PLUTO Collaboration at 27.6, 30 and 31.6 GeV shown in a scatter plot of triplicity versus thrust
e) Same data as above in the angular Dalitz plot: events with $T < 0.8$ and $T_3 > 0.9$ are shown as open circles.

The TASSO Collaboration used a generalization of sphericity[40] to define three-jet events. In this method the tracks are projected on to the event plane defined by $\vec{n}_2$ and $\vec{n}_3$ (see above). The projections are divided into three groups and the sphericity for each group S_1, S_2 and S_3 determined. The three axes and the particle assignment to the three groups are defined by minimizing the sum of S_1, S_2 and S_3. This defines the direction of the three jets and assigns the particles to these jet directions.

The distribution of the TASSO events above 27.4 GeV in the angular Dalitz plot is shown in Fig. 32c. The results of a Monte Carlo calculation for $e^+e^- \to q\bar{q}$ (Fig. 32a) and $e^+e^- \to q\bar{q}g$ (Fig. 32b) are also shown. The data clearly favours the qqg mechanismn. The TASSO observe 50 events with $\theta_3 < 160^\circ$ compared to 47 events predicted for qqg and 20 events for $q\bar{q}$.

In Fig. 33 the TASSO events are plotted versus tri-jettiness J_3. The tri-jettiness is defined as

$$J_3 = \langle p_T^2 \rangle_{in} \; / \; (1/2 \; (300 \text{ MeV/c})^2) \qquad (15)$$

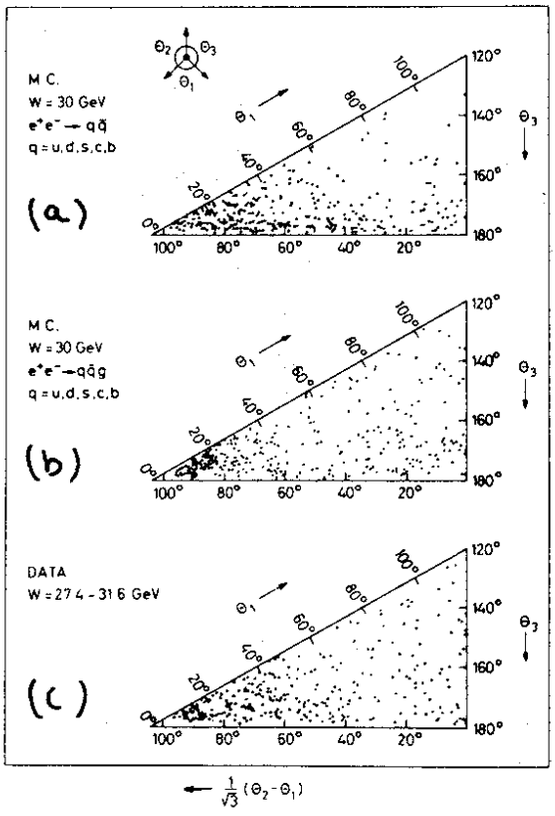

Fig. 32
Events displayed in an angular Dalitz plot with the axis determined by the generalized sphericity method.

a) Distributions expected for $e^+e^- \to q\bar{q}$

b) Distribution expected for $e^+e^- \to qqg$

c) Data obtained by the TASSO Collaboration for c.m. energies between 27.4 GeV and 31.6 GeV

where $\langle p_T^2 \rangle_{in}$ is computed for all charged tracks with respect to their assigned axis. Thus for three-jet events with a mean transverse momentum of 300 MeV with respect to the jet axis we expect to find the events clustered around $J_3 = 1$, compared with a wide distribution in J_3 in case of a flat phase space distribution. The data agree with the expectations for $e^+e^- \to q\bar{q}g$, shown as the solid line. The fit result in χ^2/degree of freedom of 2.3/5. The data disagree strongly with a phase space calculation[41] shown as the dashed line. This fit has χ^2/degree of freedom of 223/5. Thus the data are not consistent with a phase space distribution.

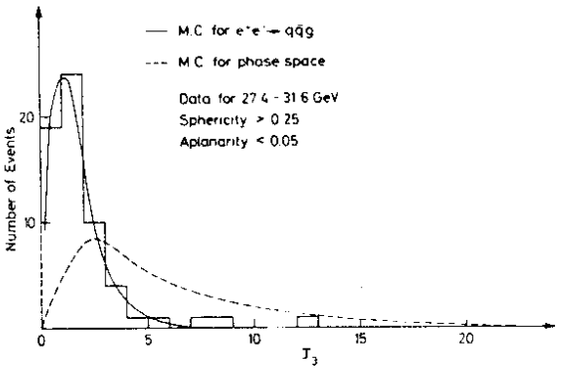

Fig. 33
Planar events ($S \geq 0.25$, $A < 0.05$) measured by the TASSO Collaboration plotted versus the tri-jettiness J_3. The M.C. predictions for $e^+e^- \to q\bar{q}g$ (solid) and for $e^+e^- \to$ hadrons according to phase space.

The MARK J group observe[5] a three-jet structure in their energy flow analysis. To extract this structure from the data they divide the energy distribution of each event into two hemisspheres by the plane containing the major and the minor axis. The narrow jet is contained in the forward hemisphere. The major, the minor and the oblateness are calculated separately for each hemisphere. To enhance effects resulting from gluon emission they select events with low thrust $T < 0.8$ and large oblateness $O > 0.1$. The accumulated energy distribution in the plane defined by the thrust and the major axis shown in Fig. 34a has a three-jet structure. The two small jets have been oriented according to size. The calculated energy distribution is in agreement with predictions based on $e^+e^- \to q\bar{q}g$ and is shown as the solid line. In Fig. 34b the accumulated energy distribution in the thrust-minor plane is shown. The flat distribution is consistent with the $q\bar{q}g$ predictions.

The remaining question is then to decide if the third jet is defined by a single particle or by a group of particles. This can be done simply by examining the events. Figs. 35 and 36 show typical candidates for three-jet events observed by the TASSO Collaboration and by the PLUTO Collaboration. For comparison also a two-jet event is shown. The main inserts shows the events viewed along the $\vec{n}_1$ direction, i.e. down onto the event plane. The three axes are

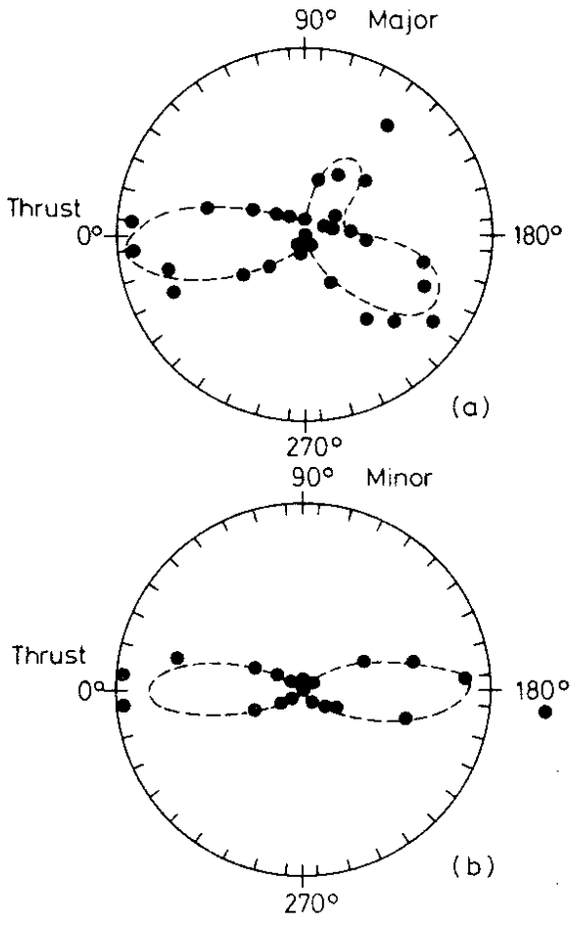

Fig. 34
a) A polar plot of the energy distribution in the plane defined by the thrust and the major axes for all events with thrust < 0.8 and oblateness > 0.1. The measurements were done by the MARK J group at c.m. energies of 27.4, 30 and 31.6 GeV. The energy value is proportional to the radial distance. The superimposed dashed line is the distribution calculated using $q\bar{q}g$ model.
b) The measured and calculated energy distribution in the plane defined by the thrust and the minor axes.

indicated by the dotted lines in the TASSO picture and by the fat bars at the border of the picture in the PLUTO event. The TASSO events contain only charged tracks, the direction of neutral tracks in the PLUTO event is indicated by dotted lines. In both events we see a clear 3-jet structure and each jet contains many tracks. In the two small insertions the events are viewed in the event plane along and transverse to the $\vec{n}_3$ direction. Viewed along the $\vec{n}_3$ direction there is a striking difference between two-jet events and three-jet events.

The TASSO group has also evaluated the transverse momentum of charged particles from three-jet events with respect to the jet axes to which they were assigned by the generalized sphericity method[40]. This distribution, $1/N\ dN/dp_T^2$, is plotted versus p_T^2 in Fig. 37. It is compared to the p_T^2 distribution found with respect to the jet axis in two-jet events at lower energies shown as the solid line. The agreement is very good and demonstrates that $\langle\sigma_g\rangle$ can be taken to be constant independent of energy, when the events at high energy are analyzed as three-jet events.

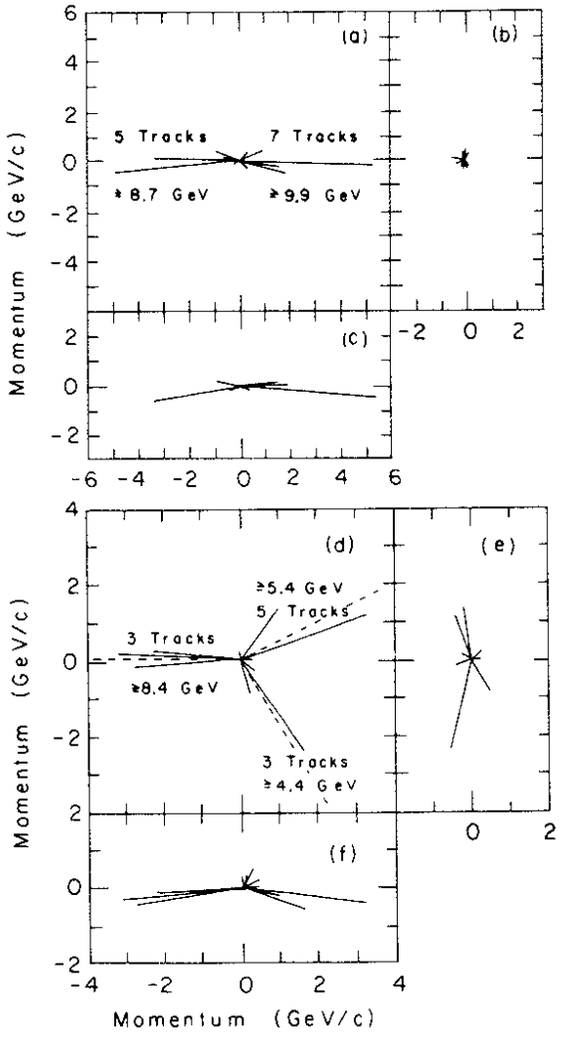

Fig. 35
Momentum space representation of a 2-jet event (a,c) and a 3-jet event (d-f) in each of three projections (a,d) = $\vec{n}_2$ - $\vec{n}_3$ plane; (b,e) = $\vec{n}_1$-$\vec{n}_2$ plane; (c,f) = $\vec{n}_1$-$\vec{n}_3$ plane. The events were measured by the TASSO Collaboration and the dotted line shows the fitted jet axis.

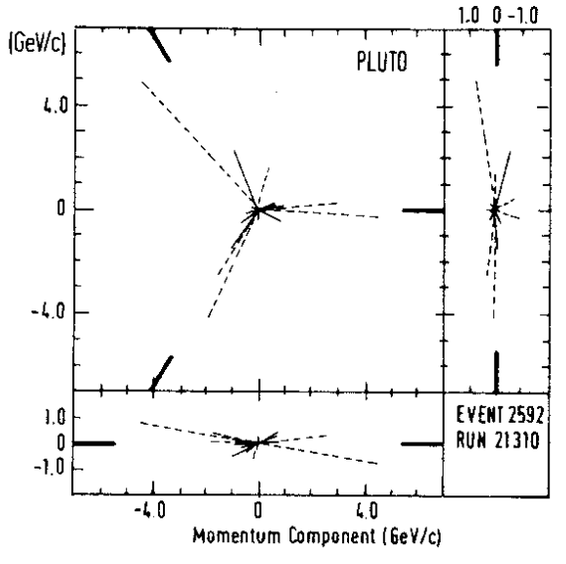

Fig. 36
Momentum vectors of an high triplicity low thrust event, measured by the PLUTO Collaboration at 31.6 GeV in c.m. The event is shown projected onto the triplicity plane (top left), onto a plane normal to the fastest jet (top right) and onto a plane containing the direction of the fastest jet (bottom). Solid and dotted lines correspond to charged and neutral particles, respectively. The directions of the jet axes are shown as the fat bars.

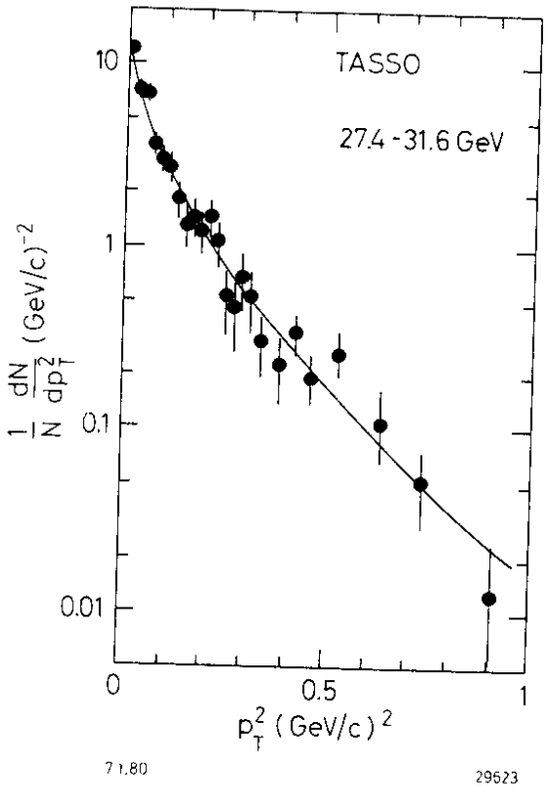

Fig. 37
The transverse momentum distribution $1/N\ dN/dp_T^2$ of the hadrons in the planar events with respect to the three axes found by the generalized sphericity method. The solid line shows the transverse momentum distribution with respect to the jet axis found in 2-jet events at lower energies. The data are from the TASSO Collaboration.

E) CONCLUSION

The naive quark-parton model does not describe the data at high energies. The data show a clear three-jet structure, which result from an initial state of three basic particles. All the properties of these events are consistent with those expected for gluon bremsstrahlung $e^+e^- \to qqg$ in QCD.

5. SEARCH FOR FRACTIONALLY CHARGED OR HEAVY STABLE PARTICLES

$e^+e^- \to q\bar{q}$ is an ideal place to look for free quarks. The JADE Collaboration[7] has searched for quarks and heavy stable particles using the dE/dx information from the drift chamber. The drift chamber measures dE/dx at 48 points along the track. To reduce the fluctuations from the Landau tail of the ionization loss the highest 20% of the measurements are ignored and the mean of the remaining 80% used. This results in a dE/dx resolution of $\pm$ 6% determined from a measurement of Bhabha scattering.

The dE/dx for each track in multihadron events are plotted in Fig. 38 versus momentum. To be accepted, the ionization must have been measured at least 30 times. Note that the threshold for an ionization measurement is set to 1/7 of the energy loss of a minimum ionizing particle emitted at 90° to the beam.

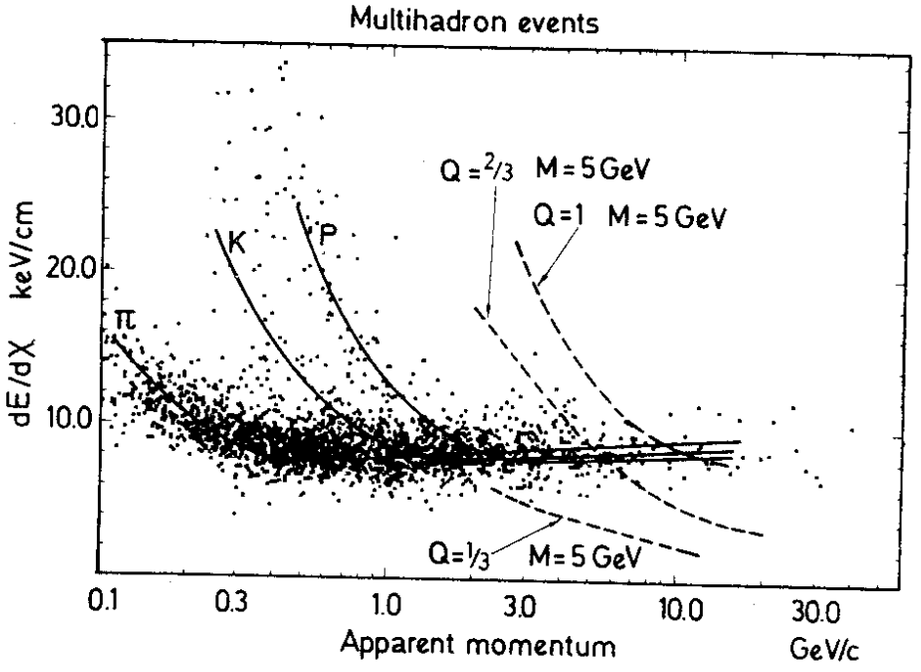

Fig. 38 - dE/dx versus apparent momentum measured in multihadron events by the JADE Collaboration. The energy loss expected for π, K, p are shown as the solid lines. The energy loss expected for fractionally charged or heavy stable particles is shown as the dotted lines.

The energy loss curves predicted for pions, kaons and protons are plotted as solid lines in Fig. 38. The energy loss curves for 1/3 e, 2/3 e particles and a stable particle of mass 5 GeV and unit charge are plotted as dotted lines. The points accumulate along the energy loss curves of the ordinary particles with no accumulation of points along the quarks or the heavy stable particle lines. The upper limits on the production cross section in the corresponding momentum ranges are listed in table V.

Table V - Upper limits ΔR on the production of fractionally charged particles and heavy particles with unit charge

Charge	Mass (GeV)	Range of true momenta GeV/c		upper limit ΔR
1/3	3	$1.5 < p < 2$		0.1
	5	$2 < p < 3$		0.1
	10	$1 < p < 7$		0.1
2/3	3	$p < 1$	$p > 3.5$	0.1
	5	$p < 2$	$p > 4$	0.1
	10	$p < 4.5$	$p > 10$	0.1
1	3	$p < 2$		0.08
	5	$p < 6$		0.08
	10	$p < 10$		0.08

The JADE Collaboration use the absence of heavy particles to set an upper limit on the lifetime τ of the B. Assuming a mass of 5 GeV, a $B\bar{B}$ production cross section of $\Delta R = 1/9$ and a flat momentum distribution of the B mesons they find $\tau < 3 \times 10^{-9}$ sec.

6. TWO PHOTON REACTIONS

Electron-positron collisions are a source of photon-photon collisions[42] as shown in Fig. 39. The mass $(-q^2)$ of the virtual photon is determined by the kinematics of the outgoing lepton. Photon-photon collisions therefore offer a unique opportunity to vary the mass of both the target and projectile over a wide range.

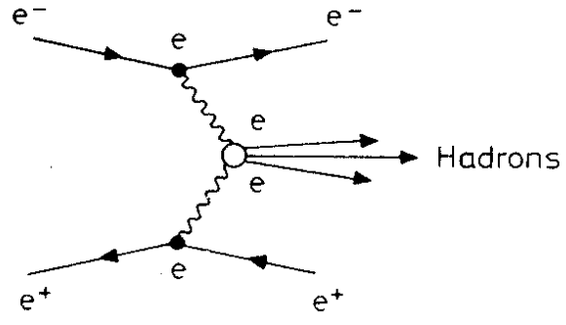

Fig. 39
Feynman graph for
$e^+e^- \to e^+e^-X$

One might investigate the whole kinematic region from collisions of two nearly real photons (hadron-hadron interaction) via deep inelastic electron-photon interactions to the collisions of two heavy photons. Unlike the annihilation process the two photon pro-

cesses will lead to a final state with two leptons, in general with high energies and at forward angles, plus hadrons with a visible energy much less than the c.m. energy. The two processes can therefore readily be separated.

The PLUTO Collaboration has reported the first results on $e^+e^- \to e^+e^-$ hadrons at high energies. The number of observed events, with the beam-gas contribution subtracted, are plotted in Fig. 40 as a function of visible energy. The distribution has two peaks,

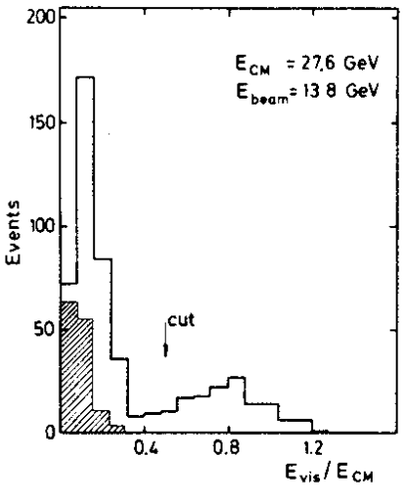

Fig. 40
Distribution of the measured energy per event (charged + neutral) measured by the PLUTO Collaboration at 27.6 GeV. The hatched area shows the energy distribution of events with a single tag in the forward detector.

one corresponding to events with a large visible energy, resulting from annihilation events, the second peak to events with low visible energy. The second peak with a very steep drop towards large visible energies is naturally explained by two photon reaction where the sharp drop is caused by the falling bremsstrahl spectrum of the interacting photons. This interpretation is reinforced by the distribution of events with a lepton in one of the forward spectrometers, which covers angles between 23 and 70 mrad.

This distribution, shown as the hatched area in Fig. 41, only lead to events with small observed energy. Thus the annihilation and the two-photon reaction are well separated by demanding an electron in the forward detector and a cut on visible energy.

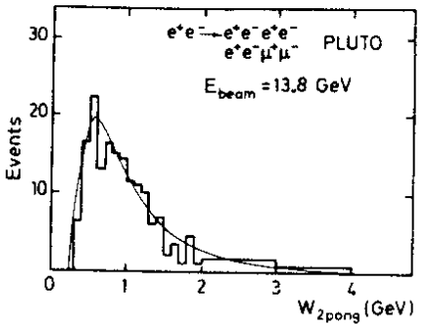

Fig. 41
Distribution of the invariant mass of two prong events in the central part of the PLUTO detector with a tag in the forward detector. The QED prediction is shown by the solid line.

The PLUTO group[10] first selected events of the type $e^+e^- \to e^+e^-$ + 2 charged prongs. This class of events will mainly be populated by the two QED reactions $e^+e^- \to e^+e^-e^+e^-$ and $e^+e^- \to e^+e^- \mu^+\mu^-$. The number of two prong events at 27.6 GeV in c.m. are plotted versus the invariant two prong mass in Fig. 41. The distribution peaks at a low invariant mass is in excellent agreement with the QED prediction shown as the solid line.

The hadronic events are also selected from the single tag class by demanding either three or more tracks in the central detector or two tracks in the central detector plus one neutral particle.

In these events the tagged photon had $\langle Q^2 \rangle \approx 0.1$ GeV^2 for beam energies of 6.5 GeV (8.5 GeV) and $\langle Q^2 \rangle = 0.4$ GeV^2 for a beam energy of about 15 GeV. The virtual photon from the untagged electron will be almost real.

The PLUTO Collaboration therefore analyze their data in terms of electron-photon scattering. The cross section for this process can be written[42] as

$$d\sigma = \Gamma_T(\sigma_T + \varepsilon \sigma_L)\, d\Omega'\, dE'\, N(E_\gamma)\, dE_\gamma. \qquad (16)$$

Γ_T and ε are respectively the flux factor and the polarization of the tagged photon. σ_T and σ_L are the total cross section for hadron production by virtual transverse and longitudinal photons. $N(E_\gamma)\, dE_\gamma$ is the spectrum of untagged photons. The values of $\sigma_T + \varepsilon\sigma_L$ extracted from the data are plotted in Fig. 42 as a function

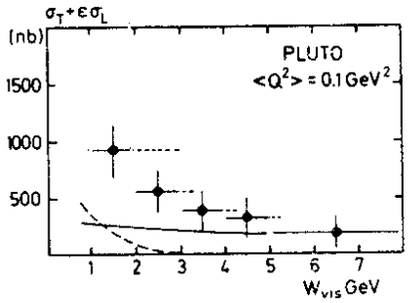

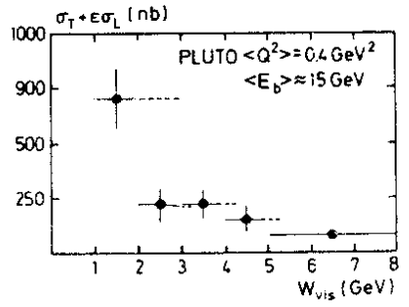

Fig. 42
Total hadronic cross section for two photons initiated events measured by PLUTO for
a) $Q^2 \sim 0.1$ (GeV/c)^2 and
b) $Q^2 \sim 0.4$ (GeV/c)^2

of the visible energy W_{vis} at $\langle Q^2 \rangle = 0.1$(GeV/c)^2 and $\langle Q^2 \rangle = 0.4$(GeV/c)^2 The range of true c.m. energies which contribute to W_{vis} is indicated by the length of the dashed horizontal bars.

Besides the statistical error there is an overall systematic uncertainty of ± 25%.

The predicted[10] cross section assuming a pure Regge behaviour of the $\gamma\gamma$ scattering extrapolated to low energies using duality arguments and factorization is shown by the solid line in Fig. 42. The estimated contribution from a point-like coupling of the photons to the quark is indicated by the dashed line. Adding the two contributions describes the energy dependence of the cross section qualitatively.

I thank A.Bäcker, R.Felst, D.Lüke, H.L.Lynch, T.Meyer, S.Orito, P.Söding, U.Timm, S.C.C.Ting, G.Wolf, S.L.Wu, G.Zobernig for data and many stimulating discussions.

REFERENCES

1. PETRA, updated version of the PETRA Proposal, DESY, Hamburg,1976
2. MARK J.Collaboration, P.Barber et al., Phys.Rev.Lett.42,1113 (1979)
   PLUTO Collaboration, Ch.Berger et al., Phys.Lett.81B, 410 (1979)
   TASSO Collaboration, R.Brandelik et al., Phys.Lett. 83B
   261 (1979)
3. B.H.Wiik, Proceedings of the International Neutrino Conference,
   Bergen, Norway, 18-22 June 1979
   R.Cashmore, Proceedings of the EPS International Conference on
   High Energy Physics, Geneva, Switzerland, 27 June-4 July 1979
   P.Söding, ibid
   G.Wolf, ibid
4. TASSO Collaboration, R.Brandelik et al., Phys.Lett. 83B,
   261 (1979)
5. MARK J Collaboration, P.Barber et al., Phys.Rev.Lett. 43,
   830 (1979)
6. PLUTO Collaboration, Ch.Berger et al., Phys.Lett. 86B,
   418 (1979)
7. JADE Collaboration, S.Orito, Proceedings of the International
   Symposium on Lepton and Photon Interactions at High Energies,
   FNAL 23-29 Aug, 1979 and DESY Report 79/77
8. A.A.Sokolov and I.M.Ternov, Sov.Phys.Doklady 8, 1203 (1964)
9. MARK J Collaboration, P.Barber et al., MIT, LNS Report Nr. 107
   Submitted to Nuclear Physics B (1979)
10. PLUTO Collaboration, Ch.Berger, invited talk, Proceedings of
    the 1979 International Symposium on Lepton and Photon Interactions at High Energies, FNAL, Aug. 23-29, 1979, FITHA 79/29
11. S.Weinberg, Phys.Rev.Lett. 19, 1264 (1967)
    A.Salam, Elementary Particle Physics, ed. N.Svartholm
    (Almkvist and Wicksell, Stockholm 1968)
12. E.H.de Groote, G.J.Gounaris and D.Schildknecht,
    Bielefeld Report, BI-TP 79/15
13. S.D.Drell, D.J.Levy, and T.M.Yan,
    Phys.Rev. 187, 2159 (1969) and Phys.Rev. D1, 1617 (1970)
14. N.Cabibbo, G.Parisi, and M.Testa, Lett.Nuovo Cimento 4, 35 (1970)
15. J.D.Bjorken and S.J.Brodsky, Phys.Rev.D1, 1416 (1970)
16. R.P.Feynman, Photon-Hadron Interactions (Benjamin,
    Reading, Mass., p. 166, 1972)

17. R.F.Schwitters et al., Phys.Rev.Lett. 35, 1230 (1975)
G.G.Hanson et al., Phys.Rev.Lett. 35, 1609 (1975)
G.G.Hanson, Proceedings of 13th Rencontre de Moriond, edited by J.Tran Thanh Van, Vol. II, p. 15 and SLAC-PUB 2118 (1978)
Ch.Berger et al., Phys.Lett. B78, 176 (1978)
18. J.Kogut and L.Susskind, Phys.Rev. D9, 697, 3391 (1974
A.M.Polyakov, Proceedings of the 1975 International Symposium on Lepton and Photon Interactions at High Energies, Stanford, Aug. 21-27, 1975
19. The first discussion on the experimental implications of gluon bremsstrahlung in e^+e^- annihilation was given by:
J.Ellis, M.K.Gaillard and G.G.Ross, Nucl.Phys. B 111, 253 (1976) - erratum B 130, 516 (1977)
20. T.A.DeGrand, Yee Jack Ng, and S.-H.H.Tye, Phys.Rev. D 16, 3251 (1977)
A.de Rujula, J.Ellis, E.G.Floratos and M.K.Gaillard, Nucl.Phys. B 138, 387 (1978)
G.Kramer and G.Schierholz, Phys.Lett. 82B, 102 (1979)
G.Kramer, G.Schierholz and J.Willrodt, Phys.Lett. 79B, 249 (1978)
P.Hoyer, P.Osland, H.G.Sander, T.F.Walsh and P.M.Zerwas, DESY 78/21 - to be published
G.Curci, M.Greco and Y.Srivastava, CERN-Report 2632-1979
G.Kramer, G.Schierholz and J.Willrodt, DESY Report 79/69
21. H.Fritzsch, M.Gell-Mann and H.Leutwyler, Phys.Lett. 47B, 365 (1973)
D.J.Gross and F.Wilczek, Phys.Rev.Lett. 30, 1343 (1973)
H.Politzer, Phys.Rev.Lett. 30, 1346 (1973)
S.Weinberg, Phys.Rev.Lett. 31, 31 (1973)
22. See J.Ellis for a review of the status of QCD in deep inelastic reactions. Proceedings of the International Neutrino Conference, Bergen, Norway 18-22 June, 1979
23. PLUTO Collaboration, Ch.Berger et al., Phys.Lett. 86B, 413 (1979)
24. JADE Collaboration, W.Bartel et al., DESY Report 79/64
25. TASSO Collaboration, R.Brandelik et al., DESY Report 79/74
26. A.Quenzer, thesis, Orsay Report LAL 1299 (1977)
A.Cordier et al., Phys.Lett. 81B, 389 (1979)
V.A.Sidorov, Proceedings of the XVIIIth International Conferenence on High Energy Physics, Tbilisi, USSR, B13 (1976)
R.F.Schwitters, Proceedings of the XVIIIth International Conference on High Energy Physics, Tbilisi, B 34 (1976)
J.Perez-Y-Jorba, Proceedings of the XIXth International Conference on High Energy Physics Tokyo, p. 277 (1978)
G.P.Murtas, Proceedings of the XIXth International Conference on High Energy Physics, Tokyo, p. 269 (1978)
PLUTO Collaboration, J.Burmester et al., Phys.Lett. 66 B, 395 (1977)
DASP Collaboration, R.Brandelik et al., Phys.Lett. 76 B, 361 (1978)

27. T.Appelquist and H.Georgi, Phys.Rev. D8, 4000 (1973)
A.Zee, Phys.Rev. D8, 4038 (1973)
G.'t Hooft, Nucl.Phys. B62, 444 (1973)
M.Dine and J.Sapirstein, Phys.Rev.Lett. 43, 668 (1979)
28. TASSO Collaboration, R.Brandelik et al., DESY Report 79/73
29. C.Bacci et al., Phys.Lett. 86B, 234 (1979)
SLAC-LBL Collaboration, G.G.Hanson, 13th Rencontre de Moriond (1978) ed. by J.Tran Thanh Van, Vol. III (1978)
PLUTO Collaboration, Ch.Berger et al., Phys.Lett. 81 B, 410 (1979) and
V.Blobel private communication
DASP Collaboration, R.Brandelik et al., Nucl.Phys. B 148, 189 (1979)
30. W.Thomé et al., Nucl.Phys. B 129, 365 (1977)
See also review by E.Albini, P.Capiluppi, G.Giacomelli, and A.M.Rossi, Nuovo Cimento 32A, 101 (1976)
31. R.Stenbacka et al., Nuovo Cimento 51A, 63 (1979)
32. W.Furmanski, R.Petronzio and S.Pokorski, Nucl.Phys. B 155, 253 (1979)
33. G.J.Feldman and M.L.Perl, Phys.Reports 33, 285 (1977)
34. R.Baier, J.Engels and B.Peterson, University of Bielefeld Report BI-TP 79/10
W.R.Frazer and J.F.Gunion, Phys.Rev. D20, 147 (1979)
35. R.D.Field and R.P.Feynman, Nuclear Phys. B 136, 1 (1978)
see also
B.Anderson, G.Gustafsen and C.Peterson, Nuclear Physics B 135, 273 (1978)
36. A.Ali, J.G.Körner, J.Willrodt and G.Kramer, Particles and Fields C1, 269 (1979) ibid 2, 33 (1979
37. E.Fahri, Phys.Rev.Lett. 39, 1587 (1977)
38. JADE Collaboration, W.Bartel et al., DESY Report 79/70
39. S.Brandt and H.D.Dahmen, Particles and Fields C1, 61 (1979)
40. S.L.Wu and G.Zobernig, Particles and Fields C2, 107 (1979)
41. The phase space calculation shown here is for a detector without neutral detection, it includes corrections for acceptance and the model is adjusted to reproduce the high multiplicity observed
42. N.Arteago Romero, A.Jaccarini and P.Kessler, C.R.Acad.Sci. B 129, 153 (1969) and
C.R.Acad.Sci. B 269, 1129 (1969)
V.E.Balakin, V.M.Budnev and I.F. Grinzburg, Zh.Eksp.Theor.Fiz.Pis'ma Red. 11, 559 (1970) (JETP Lett. 11, 338 (1970))
S.J.Brodsky, T.Kinoshita and H.Terazawa, Phys.Rev.Lett. 25, 972 (1970)
43. L.N.Hand, Phys.Rev. 129, 1834 (1963)